COMPUTATIONAL STUDIES ON THE DYNAMISM OF CHEMICAL REACTIONS OF SOME NITROGEN- AND SULFUR-CONTAINING MOLECULES

SHIN-YA TAKANE

Faculty of Engineering Science
Osaka University
1993

COMPUTATIONAL STUDIES ON THE DYNAMISM OF CHEMICAL REACTIONS OF SOME NITROGEN- AND SULFUR-CONTAINING MOLECULES

SHIN-YA TAKANE

Faculty of Engineering Science
Osaka University
1993

Preface

Recent progress of science and technology has given powerful tools to chemists. They are computers. Especially, because of the striking developments of the hardware such as a RISC (reduced instruction set computer) microchip, we can get a tiny but powerful EWS (engineering workstation) whose performance is not so different from that of the mainframe of just a few years ago. Of course, we could not forget the development of software at the same time. In the field of chemistry, numerous sophisticated programs such as the *Gaussian* series allow us to apply ab initio molecular orbital theory to chemical problems more easily.

On such a background, the field of computational chemistry has become more and more important as the third field of chemistry, in addition to theoretical and experimental chemistries. These apear to be effectively complementary to one another.

The primary aim of this thesis is to investigate the dynamical mechanisms of the reactions of some nitrogen- and sulfur-containing molecules by ab initio molecular orbital calculations. Most part of the calculations has been carried out on gigantic supercomputers, but the rest has indeed been conducted on an EWS model HP/Apollo 9000 Series model 720.

This thesis consists of two parts. Part I is concerned with nitrogen-containing molecules. The potential energy profiles are examined by ab initio molecular orbital calculations. Using the structures and the energies obtained, dynamism of the chemical reactions and the temperature dependence of rate constants are discussed. Part II is devoted to the studies of reactions of sulfur-containing molecules. The transition states of some radical reactions are investigated using ab initio calculations. Possibility of a new type of elementary reactions is suggested.

Acknowledgments

The present thesis is a collection of the author's studies which have been carried out under the direction of Professor Takayuki Fueno at Osaka University during 1986-1993. The author is pleased to acknowledge the continuing guidance and encouragement of Professor Takayuki Fueno. Without his generous support, the present studies would have never been accomplished.

He would like to express deep gratitude to Associate Professor Tadashi Okuyama, who introduced the world of sulfur chemistry to him. He is deeply grateful to Dr. Kunihisa Yoshida for his continuous encouragement.

The author thanks Dr. Keiichi Yokoyama, Dr. Masayosi Nakano, Messrs. Hiroshi Kitaike, Katsuji Miyake, Jun'ichi Kitagawa, and Mitsutaka Okumura for their active collaboration and hot discussions. He also thanks Messrs. Kazusada Takeda, Kazunobu Onishi, Takuya Sueno, Hiroshi Akagi, and other members of the Fueno Laboratory for their friendly and continuous encouragement throughout the course of his studies.

The numerical calculations were carried out on HITAC M680H and S820 computers at the Institute for Molecular Science, and on NEC ACOS S2020 and SX-2N at the Computation Center, Osaka University. The author thanks both centers for allocations of CPU time.

Finally, the author is grateful to his parents, Yasushi and Akemi Takane, for their kind encouragement and all kinds of support during the course of his studies.

Shin-ya Takane

February, 1993

Contents

General Introduction

During the past decade, the progress of both science and technology is noteworthy. Chemistry is not an exception. Its range becomes wider and wider. However, it remains unaltered that elucidation of the mechanisms of chemical reactions is one of the most important part in chemistry.

For understanding mechanisms of chemical reactions, it seems generally true that there are some steps to be taken. To begin with, we must know what the starting material (A) is and what the product (B or C) will be.

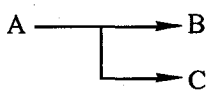

(1)

(2)

This may be achieved by product analyses, for example, by using gas chromatography or by the spectroscopic techniques, such as UV, IR, etc. At this level, the mechanism may be called a *macroscopic* mechanism.

However, in order to gain more information about the reaction, or to predict some quantities such as rate constants or product distributions, we must further know the *nature* of the elementary reactions involved, i.e., a *microscopic* mechanism. In our group, such a microscopic mechanism is termed the "dynamical mechanism" or simply "dynamism".

To discuss the dynamisms of chemical reactions, one needs information of the potential energy surfaces for the reactions. In this object, molecular orbital calculations are useful tools. Quite accurate results can often be obtained for molecules constructed of a few, typically 4 to 5, atoms.

In this thesis, we have treated two kind of molecules. One is nitrogen-containing molecules, while the other, sulfur-containing molecules. Since they are important entities related to environmental phenomena, understandings of the reactions of these molecules should be quite useful.

In part I, dynamisms of the nitrogen-containing molecules are treated. There are

four chapters.

Chapter 1 is an attempt to predict the rate constants of the reaction $NH(^3\Sigma^-) + O_2(^3\Sigma_g^-) \rightarrow NO + OH$ using the energetics obtained by ab initio MO calculations. In order to reproduce the non-Arrhenius character of the rate constants, the tunneling effects are considered.

In chapter 2, electronic structure of hydrogen nitryl HNO_2 and the path of its isomerization to HONO will be described. This molecule is the simplest case of the nitro compound. Nevertheless, it is not identified yet. Using RHF, UHF, CASSCF, and MRD-CI calculations, chemical reaction paths have been examined to understand its dynamism. The singlet excited state of HNO_2 will also be described in comparison with the isoelectronic O_3 and SO_2.

Chapter 3 describes mechanism of the reaction of the hydrogen atom with HN_3 in the gas phase. Using the same method as in chapter 1, the bimolecular rate constants for the reaction will also be examined.

In chapter 4, mechanistic features of the hydrogen abstraction reactions of $NH(^1\Delta)$ from methane and ethane will be described. $NH(^1\Delta)$ is a diradical, which has two different characters because of the presence of its degenerate valence orbitals. One is a two-configurational closed-shell type while the other, a single-configurational open-shell type. The unique role of the open-shell character of $NH(^1\Delta)$ in the reactions with methane and ethane will be demonstrated.

In part II, the mechanisms of the sulfur-containing molecules are presented. Possibilities of the bimolecular homolytic substitution reactions (S_H2) will be broached and discussed. The part consists of two chapters.

In chapter 1, dynamical mechanisms of the hydrogen abstraction and the radical substitution reactions of H_2S with some atomic species X (X = H, O, F) and those of CH_3SH with H will be described. In the case of CH_3SH + H, in particular, the results are compatible with the experimental results reported by previous workers.

In the case of $H_2S + O(^3P)$, there should exist the low-lying singlet excited state and

may well participate in the reaction since O(^{1}D) state is only 190 kJ/mol above the ground state. Under such situations, we will describe, in chapter 2, the potential energy surfaces of the reactions of H_2S with O(^{1}D), to compare them with the triplet surfaces in detail.

Part I

Dynamism of the Reactions of Some Nitrogen-Containing Molecules

Chapter 1

Theoretical Study of the Rates of the Gas-Phase Reaction of $NH(^3\Sigma^-)$ with O_2

The reaction of $NH(^3\Sigma^-)$ with $O_2(^3\Sigma_g^-)$ in the gas phase has been studied by using ab initio SCF and MRD-CI calculations. The basis set used are the 6-31G** throughout. Using the results of the molecular orbital calculations, the bimolecular rate constants were evaluated theoretically. The overall rate constants of the reaction calculated with tunneling corrections agree reasonably well with the experimental results. The apparent non-Arrhenius character of k in the temperature range 286-2000 K is rationalized most satisfactorily.

1. Introduction

Previously [1], we have studied the pathways of the reaction of NH with O_2 by using ab initio SCF and MRD-CI calculations. It was found that the reaction of $NH(^3\Sigma^-)$ with $O_2(^3\Sigma_g^-)$ should proceed through an initial association with no activation barrier:

$$NH + O_2 \longrightarrow HNOO \qquad (1)$$

Reaction (1) is followed by the rate-determining 1,3-hydrogen migration to give hydroperoxynitrene $NOOH(^1A')$, which will readily decompose into NO and OH:

$$HNOO \longrightarrow NOOH \longrightarrow NO + OH \qquad (2)$$

The net activation energy for the overall reaction

$$NH(^3\Sigma^-) + O_2(^3\Sigma_g^-) \longrightarrow NO + OH \qquad (3)$$

is calculated to be 35 kJ/mol. The calculated activation energy is somewhat too large as compared to the experimental value of 6.4 kJ/mol determined by Hack et al. in the temperature range 286-543 K [2]. Neither does it agree with the value (ca. 60 kJ/mol) estimated by Dean et al.[3] in the high temperature region (2000 K). The non-Arrhenius character of the rate constant for reaction (3) is expected to be a consequence of the tunneling effect operative in the region of the transition state.

In the present work, we examine the evaluation of the bimolecular rate constant for reaction (3) with the tunneling correction by using the one-dimensional Eckart potential [4]. The temperature dependence of the rate will be compared with the experimental results.

2. Method of calculations

2.1. Energetics

Details have already been described by Yokoyama [1]. Suffice it here just to outline the methods used. Geometry optimizations were basically carried out by the UHF SCF procedure using the Gaussian 82 program package [5]. For the ground state of HNOO(^{1}A'), multi-configuration (MC) SCF method has been adopted. In practice, we used the limited-configuration formalism in which six electrons are accommodated in six frontier orbitals with the remaining electrons frozen in the low-lying molecular orbitals. Paths of the isomerization of HNOO (^{1}A') were traced by the same MC SCF procedure. The basis sets employed are throughout the conventional 6-31G functions [6] augmented with one set each of *d* or *p* polarization functions for every atom involved.

In order to improve the energies, MRD-CI calculations were performed for all the stationary geometries located. The TABLE MRD-CI program furnished by Buenker [7, 8] was used. To obtain an estimated full CI value E_{CI}, the extrapolation routine [9], and the multi-reference type of Davidson-Langhoff corrections [10] were followed .

2.2. Tunneling Correction

In this section, simple tunneling corrections for the rate constants will be described. The method used is based almost entirely on Johnston's formulation [11].

In quantum mechanics, a particle with energy greater than the barrier height may be reflected, and a particle with energy E less than the barrier height has a finite chance of appearing on the other side of the barrier with the same energy E. This non-classical barrier penetration is called "tunneling effect". Since exact quantum-mechanical treatments of general chemical reactions are difficult or even impossible, we should recourse to effective models which can be applied to general cases. To this end, the following assumptions are commonly used:

(a) The barrier is one-dimensional, i.e., the potential $V(x)$ is only a function of a reaction coordinate, x.

(b) The mass of the particle m is constant during the process (i.e. is independent of x). Furthermore, it is often used the mass of the particle as proton or deuterium.

As the one-dimensional potential, the Eckart potential [4] is used. The Eckart potential is a realistic function which changes smoothly and continuously and for which Schrödinger equation can be solved exactly. The explicit form is

$$V(y) = -\frac{Ay}{1-y} - \frac{By}{(1-y)^2}, \qquad y = -\exp(2\pi x/L) \tag{4}$$

and the barrier is illustrated in Fig. 3. The Eckart-potential constants A, B, and L should satisfy the following relations

$$\begin{aligned} A &= V_1 - V_2 \\ B &= (V_2^{1/2} + V_1^{1/2})^2 \\ \frac{L}{2\pi} &= \left(\frac{-2}{F^*}\right)^{1/2}\left(\frac{1}{V_1^{1/2}} + \frac{1}{V_2^{1/2}}\right)^{-1} \end{aligned} \tag{5}$$

where F^* is the force constant (negative) of $V(y)$ at the barrier top. The tunneling correction factor Γ is given by

$$\Gamma = \frac{e^{V_1/kT}}{kT}\int_0^\infty \kappa(E)e^{-E/kT}dE \tag{6}$$

where $\kappa(E)$ is the one-dimensional penetration probability at a given kinetic energy E (Appendix).

3. Results and Discussion

3.1. Geometries and CI energies

Since the results have already been reported in detail by Yokoyama [1], we will here summarize them only briefly.

Figure 1 shows the geometries of *cis*-HNOO, hydroperoxynitrene (**2**), and the transition state (TS2) for the isomerization (**1** → **2**), optimized by the 6-electron-6-orbital MCSCF procedure. The MRD-CI results of the overall potential surface of the reaction NH+ O_2 is illustrated in Fig. 2. The binding energy of cis-HNOO (**1**) in the ground state is 48 kJ/mol. Therefore, the most favorable pathway of the HNOO decomposition, which involves the intermediacy of hydroperoxynitrene (**2**), is predicted to have a net activation barrier height of 26 kJ/mol against the initial binary system $NH(^3\Sigma^-) + O_2(^3\Sigma_g^-)$. When vibrational zero-point energy corrections are made, the binding energy is E_0 = 27 kJ/mol while the activation energy for reaction (2) comes out to be V_1 = 62 kJ/mol. The net activation energy is therefore $E_0^{\ddagger} = V_1 - E_0$ = 35 kJ/mol.

3.2. Rate Constants

The overall reaction of our interest can be schematically represented as follows:

$$NH(^3\Sigma^-) + O_2(^3\Sigma_g^-) \underset{k_{-1}}{\overset{k_1}{\rightleftharpoons}} [HNOO]^* \xrightarrow{k_2} NO + OH \qquad (7)$$

where $[HNOO]^*$ is the vibrationally hot adduct and where k_1 is a bimolecular rate constant while k_{-1} and k_2 are the unimolecular rate constants. Under the assumption that the second step (k_2) is rate-determining, the overall second-order rate constant k can be expressed as

$$k = k_1 (k_2 / k_{-1}) / [1 + (k_2 / k_{-1})] \qquad (8)$$

Since the initial association has no activation barrier, k_1 will be given by

$$k_1 = (1/g_{NH}g_{O_2})Z \tag{9}$$

where g_{NH} and g_{O2} are the electronic degeneracy factors of NH and O_2, respectively, both being 3 in the present instance, and where Z is the collision frequency. By assuming a classical collision diameter of 3.0 Å, k_1 is approximated to be $8.620 \times 10^{11}\, T^{1/2}$ $cm^3mol^{-1}s^{-1}$. The rate constant ratio k_2 / k_{-1} is considered to be governed not only by the difference in the relevant activation barrier heights but by the tunneling factor Γ involved in k_2. We here assume naively that

$$k_2 / k_{-1} = \Gamma e^{-\Delta E_0^{\ddagger} / RT} \tag{10}$$

as an upper bound.

In evaluating the tunneling correction factor Γ at the varying temperature, we have adopted Johnston's method [11], which has already been described in a previous section. The tunneling correction factor Γ can be now expressed as

$$\Gamma = \frac{e^{V_1/RT}}{RT} \int_{E_0}^{\infty} \kappa(E)\, e^{-E/RT} dE \tag{11}$$

In the present instance, V_1 and V_2 are 62 and 235 kJ/mol, respectively, and $E_0 = 27$ kJ/mol. F^* to be used in the evaluation of $\kappa(E)$ is related to the imaginary frequency $\nu^{\ddagger}$ of the vibrational normal mode responsible to the motion of the hydrogen atom at TS2. The frequency obtained by the vibrational analysis of TS2 is $\nu^{\ddagger} = 2243i$ cm^{-1}

The Γ values at various temperatures were calculated from eq. (11) by numerical integration on a computer. The rate constants k calculated from eqs. (8) - (10) by use of these Γ values are shown in Fig. 4. Effects of the tunneling are seen to be enormous at lower temperatures. The calculation results agree reasonably well with the experimental results reported by Hack et al.[2]. Further, the calculated curve fits both

the experimental data obtained by Zetsch and Hansen at 296 K [12] and the value estimated by Dean et al. at 2000 K [3]. The apparent non-Arrhenius character of k can be rationalized most satisfactorily.

4. Conclusions

The bimolecular rate constants k calculated for the overall reaction of $NH(^3\Sigma^-) + O_2(^3\Sigma_g^-)$ with the tunneling corrections based on Johnston's method reproduce the non-Arrhenius variation of k observed over the temperature range 286-2000 K.

Appendix

When eq. (4) is inserted in the Schrödinger equation, exact solutions can be obtained and exact values derived for the permeability. A particle of mass m and energy E approaching the barrier is characterized by the relations

$$\nu^* = (1/2\pi)(-F^*/m)^{1/2} \tag{A1}$$

$$\alpha_1 = 2\pi V_1/h\nu^* \tag{A2}$$

$$\alpha_2 = 2\pi V_2/h\nu^* \tag{A3}$$

$$\xi = E/V_1 \tag{A4}$$

Using these values, the one-dimensional penetration probability $\kappa(E)$ is expressed as

$$\kappa(E) = 1 - \frac{\cosh 2\pi(a - b) + \cosh 2\pi d}{\cosh 2\pi(a + b) + \cosh 2\pi d} \tag{A5}$$

where

$$2\pi a = 2[\alpha_1 \xi]^{1/2}\left(\frac{1}{\alpha_1^{1/2}} + \frac{1}{\alpha_2^{1/2}}\right)^{-1} \tag{A6}$$

$$2\pi b = 2[\alpha_1 \xi - (\alpha_1 - \alpha_2)]^{1/2}\left(\frac{1}{\alpha_1^{1/2}} + \frac{1}{\alpha_2^{1/2}}\right)^{-1} \tag{A7}$$

$$2\pi d = 2[\alpha_1 \alpha_2 - 4\pi^2/16]^{1/2} \tag{A8}$$

When d is imaginary, the function $\cosh 2\pi|d|$ in eq. (A5) becomes $\cos 2\pi|d|$.

Under normal conditions, the particles seem to be in thermal equilibrium impinging on a barrier. Therefore, the simplest form of the energy distribution in such a stream is given by

$$\frac{dN}{N} = \frac{1}{kT} e^{-E/kT} dE \tag{A9}$$

in which dN/N is the fraction of particles having energies between E and $E + dE$.

If J_0 is the total flux of particles striking the left-hand side of the barrier, the rate J at which particles appear on the right-hand side of the barrier is given by

$$J = \frac{J_0}{kT}\int_0^\infty \kappa(E)e^{-E/kT}dE \tag{A10}$$

In classical mechanics, since $\kappa(E) = 0$ for $E < V_0$ and $\kappa(E) = 1$ for $E > V_0$, where V_0 is the potential energy at the top of the barrier, the classical rate J_c is

$$J_c = \frac{J_0}{kT}\int_{V_0}^\infty e^{-E/kT}dE = J_0 e^{-V_0/kT} \tag{A11}$$

By combining eqs. (A10) and (A11) we can obtain a tunnel correction Γ, which is the ratio of the quantum-mechanical rate to the classical rate, i.e.,

$$\Gamma \equiv \frac{J}{J_c} = \frac{e^{V_0/kT}}{kT}\int_0^\infty \kappa(E)e^{-E/kT}dE \tag{A12}$$

References

[1] K. Yokoyama, Doctoral Dissertation, Osaka University (1991).

[2] W. Hack, H. Kurzke, and H. Gg. Wagner, J. Chem. Soc. Faraday Trans. 2, **81**, 949 (1985).

[3] A. M. Dean, M. S. Chou, and D. Stern, Int. J. Chem. Kinet., **16**, 633 (1984).

[4] C. Eckart, Phys. Rev., **35**, 1303 (1930).

[5] J. S. Binkley, M. J. Frisch, D. J. DeFrees, K. Raghavachari, R. A. Whiteside, H. B. Schlegel, and J. A. Pople, GAUSSIAN 82, Carnegie-Mellon University, Pittsburgh, PA (1984); IMS version registered by N. Koga.

[6] W. J. Hehre, R. Ditchfield, and J. A. Pople, J. Chem. Phys., **56**, 2257 (1972); P. C. Hariharan and J. A. Pople, Theor. Chim. Acta, **28**, 213 (1973).

[7] R. J. Buenker, *Studies in Physical and Theoretical Chemistry*, vol. 21., ed. by R. Carbo, Elsevier, Amsterdam, pp. 17-34 (1982).

[8] R. J. Buenker and R. A. Phillips, J. Mol. Struct. (Theochem), **123**, 291 (1985).

[9] R. J. Buenker and S. D. Peyerimhoff, Theor. Chim. Acta, **35**, 33 (1974).

[10] S. R. Langhoff and E. R. Davidson, Int. J. Quant. Chem., **8**, 61 (1974).

[11] H. S. Johnston, *Gas Phase Reaction Rate Theory*, Ronald Press, New York, pp. 40 (1966).

[12] C. Zetzsch and I. Hansen, Ber. Bunsen-Ges. Phys. Chem., **82**, 830 (1978).

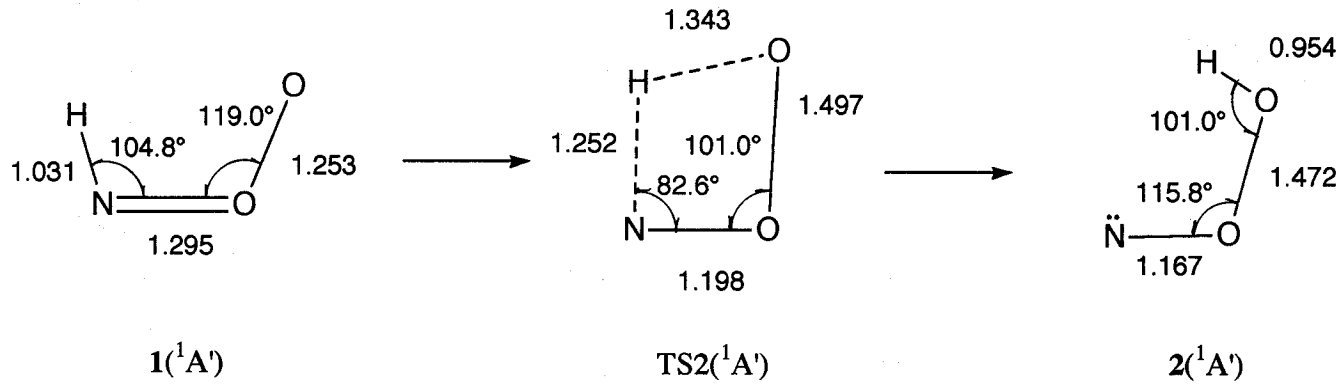

$\mathbf{1}(^1A')$ TS2($^1A'$) $\mathbf{2}(^1A')$

Figure 1. Optimized geometries of cis-HNOO (**1**), the transition state (TS2), and NOOH (**2**). The bond lengths are given in units of Å.

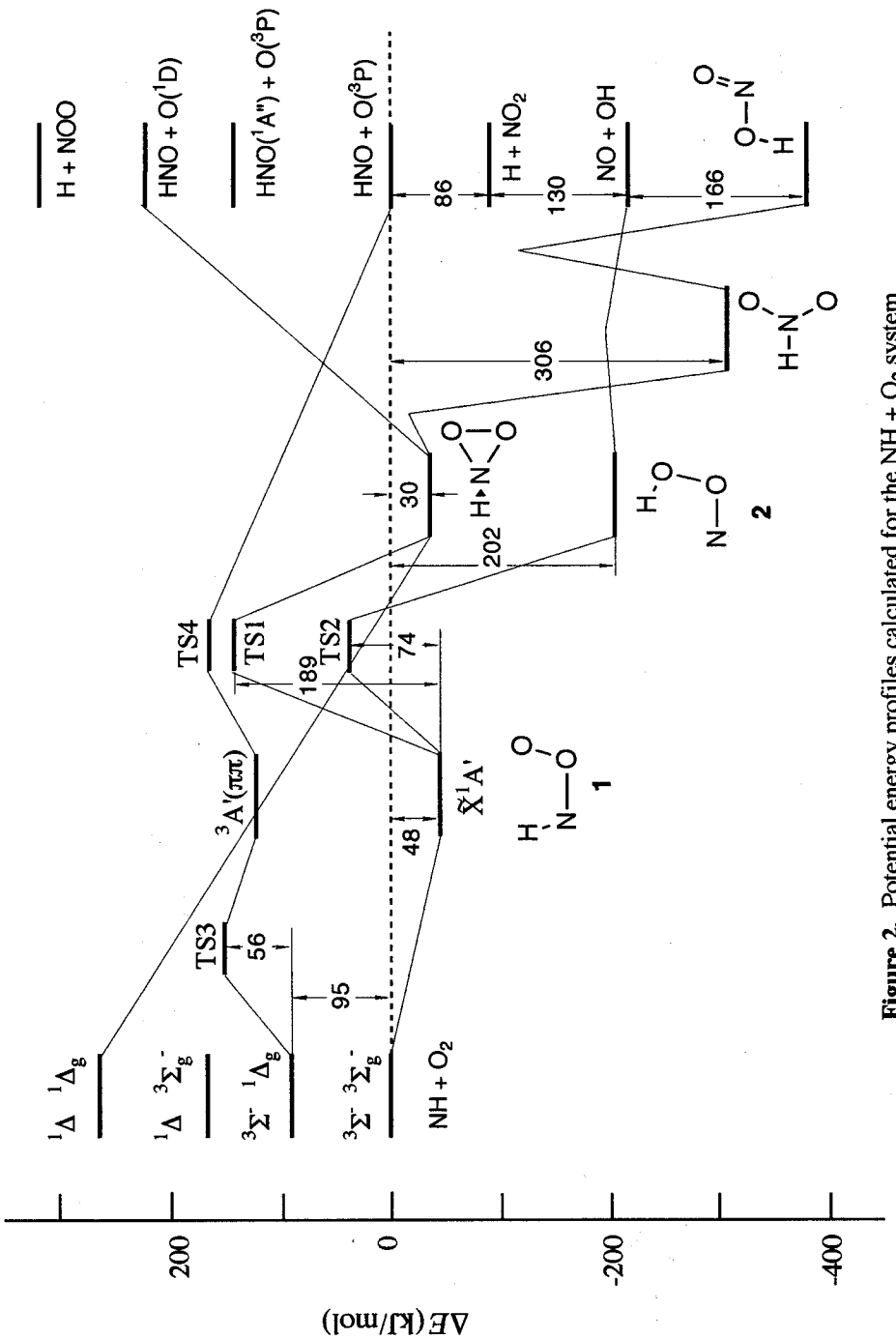

Figure 2. Potential energy profiles calculated for the NH + O_2 system. The energy levels are based on the E_{CI} values. The energy gaps indicated are given in units of kJ/mol.

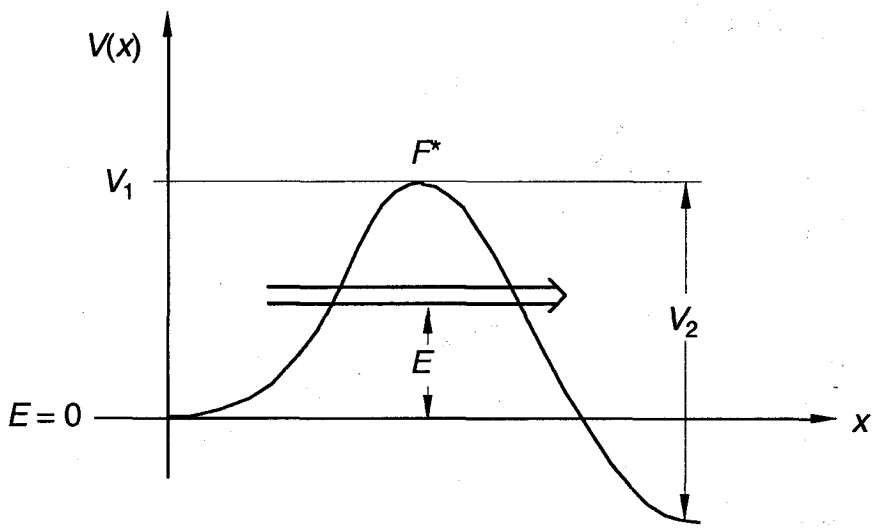

Figure 3. One-dimensional Eckart potential.

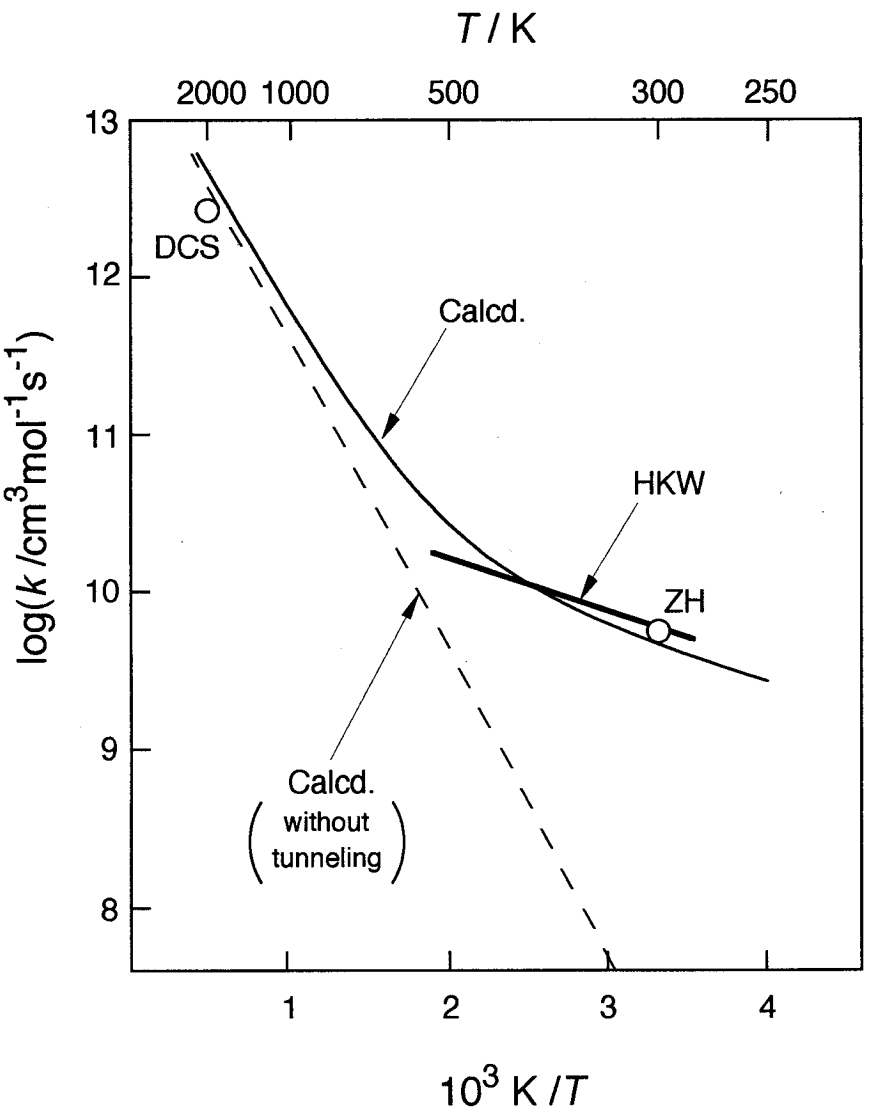

Figure 4. Rate constants for the reaction $NH(^3\Sigma^-) + O_2(^3\Sigma_g^-) \rightarrow NO + OH$. *Full line*, calculated with the tunneling correction; *broken line*, calculated without the tunneling correction. Experimental data: ZH at 296 K [12]; HKW in the temperature range 286-543 K [2]. Estimated value: DCS at 2000 K [3].

Chapter 2

Electronic Structure and the Hydrogen-Shift Isomerization of Hydrogen Nitryl HNO_2

Electronic structure of hydrogen nitryl HNO_2, a yet not identified entity, and the path of its possible isomerization to *trans*-HONO have been investigated by ab initio SCF and MRD-CI computations using the 6-31G** basis set. HNO_2 is C_{2v}-symmetric and its ground state ($^1A_1$) is less stable than *trans*-HONO by 66 kJ/mol (with the SCF vibrational zero-point energy correction). The lowest two excited singlet states ($^1A_2$ and $^1B_1$) are nearly degenerate, their vertical excitation energies being predicted to be 4.8 eV. The isomerization path is traced by the CASSCF procedure and the activation barrier height is evaluated by the CI treatment. HNO_2 in its ground state isomerizes to *trans*-HONO by maintaining the planar (C_s-symmetric) structure. The activation energy is calculated to be 171 kJ/mol, which is clearly lower than the calculated H-N bond energy (253 kJ/mol). The transition state seems to be more adequately described as an interacting system of proton and the nitrite anion rather than as a pair of two fragment radicals.

1. Introduction

In our previous work [1], we investigated the gas-phase reaction of NH with O_2 by the ab initio method. It was found that the reaction between $NH(^3\Sigma^-)$ and $O_2(^3\Sigma_g^-)$ should proceed by an initial association giving a chain intermediate HNOO ($^1A'$):

$$NH(^3\Sigma^-) + O_2(^3\Sigma_g^-) \longrightarrow HNOO \qquad (1)$$

By contrast, the reaction between $NH(^1\Delta)$ and $O_2(^1\Delta_g)$ should be a concerted cycloaddition to give a cyclic HNO_2. It will easily isomerize into nitrous acid HONO via an acyclic HNO_2(**1**) of the C_{2v} symmetry [2]:

$$NH(^1\Delta) + O_2(^1\Delta_g) \longrightarrow \underset{\textbf{1}}{\text{H—N(O)O}} \longrightarrow \underset{\textbf{1}}{\text{H—N(O)O}} \qquad (2)$$

$$\textbf{1} \longrightarrow \underset{\textbf{2}}{\text{HONO}} \qquad (3)$$

The singlet species **1**, which we here refer to as hydrogen nitryl, is the branched isomer of nitrous acid **2** and should be the simplest possible nitro compound. It has never been identified experimentally so far. The challenge to identify this isomer was first made by Jones et al.[3], who observed no indication of its contribution in the IR spectra of gaseous nitrous acid. It could also be one of the transient intermediates of the well-known gas-phase reaction of the H atom with NO_2 to produce the NO and OH radicals [4-8]. Guillory et al.[9] carried out IR spectroscopic studies of the products of the H + NO_2 reaction conducted by the matrix isolation technique, to observe *cis*- and *trans*- HONO alone; no trace of the nitro form (**1**) was discernible.

Hydrogen nitryl (**1**) may be used as a convenient prototype for existing nitro compounds in assessing their thermochemical stabilities relative to the chain isomers

[10]. To the best of our knowledge, however, there has been no explicit study to trace the path of its isomerization pathway (reaction (3)). Elucidation of the intrinsic path of reaction (3) by ab initio SCF and CI calculations is the primary concern of the present investigation. We will also attempt theoretical predictions of the vertical singlet excitation energies of **1**.

2. Method of calculations

The path of isomerization was traced first by the RHF SCF procedure, using the Gaussian 86 program package [11]. The atomic orbital functions used in this study are primarily the 6-31G** basis set [12]. The transition state (TS) was located and verified by the vibrational analysis. For all the stationary points on the isomerization path (i.e., HNO_2, TS, and *trans*-HONO), CASSCF (8 electrons in 6 orbitals) calculations [13] were then performed to improve their geometries. For the fragment radicals, the unrestricted Hartree-Fock (UHF) method was used.

At all the optimized geometries, multi-reference double-excitation configuration-interaction (MRD-CI) calculations were carried out. The Table CI program [14, 15] furnished by Buenker was used. The configuration-selection and extrapolation routines were followed [16]. The maximal dimension of the configuration space used was 8000-10,000. The extrapolated CI energies were all subjected to the Langhoff-Davidson corrections [17], to estimate the full CI limit values E_{CI}. To determine the reference (main) configurations, we preliminarily performed a single-reference SD-CI calculation at each state . The configurations whose contributions $|C_i|^2$ to a state under consideration exceeded 0.3 % were then regarded as the reference configurations. In this manner, the total number of the reference configurations adopted were typically 3 to 5, and the total sum of the weights $|C_i|^2$ of the reference configurations were at least 0.90.

In calculating the vertical excitation energies, the lowest three roots of each

irreducible representation were evaluated in a similar manner as above. The total number of the reference configurations ranged from 12 to 22 in these multi-root calculations.

3. Results

3.1 Electronic structure

The C_{2v} geometry for hydrogen nitryl (**1**) optimized at the RHF level is shown in Figure 1-a. The reference configurations adopted in the subsequent CI calculation are shown in Table 1, together with their contribution weights (squared weights, $|C_i|^2$).

As can be seen in Table 1, the contribution of the electronic configuration

$$A_1; (1a_1)^2 \ldots (1b_1)^2 (4b_2)^2 (6a_1)^2 (1a_2)^2$$

to the ground state of HNO_2 (**1**) amounts to 0.87. The contribution of a configuration arising from the transition $(1a_2)^2 \rightarrow (2b_1)^2$ (i.e., the $\pi \rightarrow \pi^*$ double excitation) is as large as 0.025. The result clearly indicates the necessity of a multi-configurational treatment for a more adequate representation of the ground state geometry.

Under such circumstances, the CASSCF (8-6, i.e., eight active electrons distributed in six orbitals) method was used to further optimize the geometry. The result is shown in Figure 1-b. It can be seen that the N-O bond length obtained at the CASSCF method is considerably longer than that at the RHF SCF level , while the remaining parameters are little altered.

At the CASSCF optimized geometry, several vertical singlet excitation energies of HNO_2 were evaluated by the multi-root CI calculations. The basis sets used there were the 6-31G** functions augmented with a single primitive Rydberg s-type function (ζ = 0.028) on the N atom. All the molecular orbitals used for these calculations were those of the ground-state HNO_2 consistently. The dominant electron configurations for the

lowest-lying excited states that belong to different irreducible representations of the C_{2v} point group are all such that accommodate an electron in the $2b_1$ orbital:

$$B_1;\ \ldots(1b_1)^2(4b_2)^2(6a_1)^1(1a_2)^2(2b_1)^1 \qquad (6a_1)\rightarrow(2b_1)$$

$$B_2;\ \ldots(1b_1)^2(4b_2)^2(6a_1)^2(1a_2)^1(2b_1)^1 \qquad (1a_2)\rightarrow(2b_1)$$

$$A_2;\ \ldots(1b_1)^2(4b_2)^1(6a_1)^2(1a_2)^2(2b_1)^1 \qquad (4b_2)\rightarrow(2b_1)$$

The vertical excitation energies ΔE_{CI}^{vert} calculated for a few excited states belonging to each irreducible representation are collected in Table 2. For the sake of comparison, the ΔE_{CI}^{vert} values calculated for O_3 and SO_2 [18] as isoelectronic homologs are included in Table 2.

As is shown in Table 2, the lowest excited singlet states are $1A_2$ and $1B_1$, whose vertical excitation energies are both 4.8 eV (the difference being less than 10^{-2} eV) at the CASSCF geometries. The trend is qualitatively similar to the case of ozone, where the vertical excitation energies are 2.2 and 2.3 eV, respectively [18]. The third-lowest excited state is calculated to be the $1B_2$ state (7.5 eV), a result which is in line with the case of SO_2. In the case of O_3, the third-lowest is the $2A_1$ state (4.5 eV), which arises from the double transition $(4b_2)^2\rightarrow(2b_1)^2$ and hence accommodates a total of six electrons in its π-orbitals. As for the A_1 states of HNO_2, the second and the third roots are nearly degenerate (10.5 and 10.6 eV). The two excited A_1 states for SO_2 are also nearly degenerate (8.7 and 9.0 eV). The general pattern of electronic excitations for HNO_2 thus resembles more closely that for SO_2 rather than for O_3.

3.2 Isomerization path

The SCF and CASSCF optimized geometries of the transition state (TS) for the isomerization of HNO_2 (**1**) to *trans*-HONO (**2**) are shown in Figure 1, together with the geometries optimized for *trans*-HONO. The experimental geometry data for *trans*-HONO are given in parentheses. Clearly, the CASSCF method gives the geometry of

trans-HONO in better agreement with the experimental structure than does the RHF SCF method.

Before obtaining the TS geometries given in Fig. 1, preliminary calculations using the STO-3G and 4-31G basis sets were carried out. The results are summarized in Table 3. At the RHF/STO-3G level, the geometry is *not* planar-symmetric, the dihedral angle $<O^4NO^3H$ being 114.0°. By contrast, at both the 4-31G and 6-31G** levels, the structures conformed to the planar (C_s) symmetry. It has been confirmed that the transition state TS geometry provides one single imaginary frequency ($2640i\,cm^{-1}$) at the RHF/6-31G** level. The RHF activation barrier height obtained was $\Delta E^{\ddagger} = 278$ kJ/mol. At the CASSCF/6-31G** level, little change in geometry has been observed except for the N-O^3 bond length, which is slightly longer than the RHF result. The activation barrier height at this level was calculated to be 269 kJ/mol.

Results of MRD-CI calculations at the CASSCF optimized geometries are summarized in Table 4. The total energies of the fragment radical pairs (i.e., H + NO_2 and NO + OH) are also listed. In calculating the CI energies for these latter entities, special cautions have been exercised. Thus, in order to minimize the possible size inconsistency in the evaluation of the electron correlation effects, the fragment radical pairs (H + NO_2 and NO + OH) were treated as supermolecules separated by 20.0 Å.

According to the E_{CI} data given in Table 4, HNO_2 (**1**) is less stable than *trans*-HONO (**2**) by 62 kJ/mol. The TS for isomerization lies 253 kJ/mol above **2**. The activation barrier height for the isomerization of **1** to **2** is thus calculated to be $\Delta E_{CI}^{\ddagger} = 191$ kJ/mol. When corrections for the vibrational zero-point energy at the SCF level are included, the relative energy between HNO_2 (**1**) and *trans*-HONO (**2**) comes out to be $\Delta E_0 = 66$ kJ/mol, and the activation energy for the process **1**→**2** is reduced to $\Delta E_0^{\ddagger} = 171$ kJ/mol.

The overall potential energy profile based on the E_{CI} results calculated for the HNO_2 - HONO system is diagrammatically shown in Fig. 2. The energy gaps obtained by correcting for the vibrational zero-point energy are given in parentheses. The total CI energies of the H + NO_2 and the NO + OH systems relative to HONO are $\Delta E_{CI} = 354$

and 198 kJ/mol, respectively. Upon corrections for the vibrational zero-point energies, the bond dissociation energies of *trans*-HONO corresponding to the processes

$$\textit{trans}\text{-HONO} \rightarrow H + NO_2 \quad (4)$$

$$\textit{trans}\text{-HONO} \rightarrow NO + OH \quad (5)$$

come out to be $\Delta E_0 = 319$ and 175 kJ/mol, respectively. These results are in reasonable agreement with the respective experimental thermochemical data of $\Delta H^\circ = 325$ and 201 kJ/mol [19]. The calculated H-N bond energy for HNO_2 is $\Delta E_0 = 253$ kJ/mol.

4. Discussion

As has already been mentioned, the initial step of the reaction between H atom and NO_2 is a radical association. For this step there can exist two pathways distinct with respect to the position where the H atom attacks NO_2.

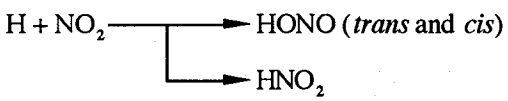

One pathway is such that the H atom attacks one of the O atoms of NO_2, thus forming *cis*- or *trans*-HONO, while in the other the H atom attacks the N atom to form the symmetric HNO_2. Neither pathway should have an activation barrier. Guillory et al.[9] have mentioned that since the SOMO of NO_2 is more localized on the N atom as discussed by Walsh [20], the H atom should attack the N atom more favorably than the O atoms. However, their experimental results indicated that the HNO_2 (nitro form) did not occur to any significant extent. They concluded that this reaction should proceed through a "hot molecule", HNO_2*, which would "fly apart" after a short but finite lifetime, or possibly through an activated complex similar in structure to nitrous acid. Our results of calculation (Fig. 2) indicate that although the isomerization from HNO_2

to *trans*-HONO possesses a large barrier height (171 kJ/mol), it is 82 kJ/mol *lower* than the N-H bond energy (253 kJ/mol) of HNO_2. Thus, the reaction might well proceed to trans-HONO via the "hot HNO_2*". Alternatively, it can be said that HNO_2 is located in a moderately deep well of the potential surface. Therefore, if the hot HNO_2* could be stabilized effectively, one could well identify or even isolate this intriguing nitro compound.

It is of interest to compare our present results with those for other well-known nitro compounds. On the basis of the MNDO calculations, Dewar and co-workers [21] predicted that the barrier height of the isomerization of nitromethane to methyl nitrite is $\Delta E^{\ddagger}$ = 197 kJ/mol, which is 61 kJ/mol lower than the energy of the C-N bond rupture. The results were taken as a theoretical justification of the observation by Benson et al.[22], who reported that the thermal decomposition of nitromethane tended to lead to CH_3O + NO in prevalence over CH_3 + NO_2. Lee and co-workers [23] estimated the barrier height to be 232 kJ/mol by combining the results of their infrared multiple-photon dissociation (IRMPD) experiments with the RRKM theoretical considerations. The estimated barrier height lend support to the theoretical prediction made by Dewar et al.[21]. The results of the present ab initio study for the case of HNO_2 are basically in harmony with those of Dewar's semiempirical study on CH_3NO_2.

On the other hand, recent ab initio theoretical studies by McKee based on the CASSCF and MR-CI methods [24] conclude that the isomerization barrier is 42 kJ/mol *higher* than the energy level for CH_3 + NO_2. Saxon and Yoshimine [25] have investigated a similar isomerization of NH_2NO_2 using MCSCF and MR-CI methods, to conclude that the barrier height is only 4 kJ/mol lower than the level for the NH_2 and NO_2 radical pair. Both studies have indicated that the transition states of the isomerization are characterized as interacting fragment radicals placed at a considerably large separation (~2 Å). In the case of HNO_2 of our concern, however, the transition state is not like such radical pairs as in these cases; as has been shown in Table 3, little change in the TS geometry is noticeable between the SCF and the CASSCF treatments.

Results of the MRD-CI calculations for TS (Table 1) provide virtually no indication of the diradical character. The situation remains unaltered when the geometry of the CASSCF/6-31G** was used in the CI calculation. The Mulliken population on the H atom at the TS in our calculation is as low as 0.513, a result which indicates an ion-pair character to be represented as H^+ --- NO_2^-. The trend is in line with the RHF-like character of our TS for the isomerization reaction.

References

[1] T. Fueno, K. Yokoyama, and S. Takane, Theor. Chim. Acta, **82**, 299 (1992).

[2] C. F. Melius and J. B. Binkley, ACS Symp. Ser. 249 (1984), cited in ref. 4.

[3] L. H. Jones, R. M. Badger, and G. E. Moore, J. Chem. Phys., **19**, 1599 (1951).

[4] M. A. A. Clyne and B. A. Thrush, Trans. Faraday Soc., **57**, 2176 (1961).

[5] A. McKenzie, M. F. R. Mulcahy, and J. R. Steven, J. Chem. Soc. Faraday Trans. I, **70**, 549 (1974).

[6] J. E. Spencer and G. P. Glass Chem. Phys., **15**, 35 (1976).

[7] H. Gg. Wagner, U. Welzbacher, and R. Zellner, Ber. Bunsenges. Phys. Chem., **80**, 1023 (1976).

[8] A. C. Luntz, IBM Res. Develop., **23**, 596 (1979).

[9] W. A. Guillory and C. E. Hunter, J. Chem. Phys., **54**, 598 (1971).

[10] S. Nakamura, M. Takahashi, R. Okazaki, and K. Morokuma, J. Am. Chem. Soc., **109**, 4142 (1987).

[11] M. J. Frisch, J. S. Binkley, H. B. Schlegel, K. Raghavachari, C. F. Melius, R. L. Martin, J. J. P. Stewart, F. W. Bobrowicz, C. M. Rohlfing, L. R. Kahn, D. J. DeFrees, R. Seeger, R. A. Whiteside, D. J. Fox, E. M. Fleuder, S. Topiol, and J. A. Pople, GAUSSIAN 86, Carnegie-Mellon Quantum Chemistry Publishing Unit. Pittsburgh (1984); IMS version registered by N. Koga, S. Yabushita, K. Sawabe, and K. Morokuma.

[12] W. J. Hehre, L. Radom, P. v. R. Schleyer, J. A. Pople, *Ab Initio Molecular Orbital Theory*, Wiley, New York, pp. 82 (1986).

[13] M. Dupuis, J. D. Watts, H. O. Villar, and G. J. B. Hurst, HONDO ver. 7.0 QCPE #544 (1987), available from Indiana University.

[14] R. J. Buenker, *Studies in Physical and Theoretical Chemistry*, vol. 21, R. Carbo, ed., Elsevier, Amsterdam, pp17-34 (1982).

[15] R. J. Buenker and R. A. Phillips, J. Mol. Struct. (Theochem), **123**, 291 (1985).

[16] R. J. Buenker and S. D. Peyerimhoff, Theor. Chim. Acta, **35**, 33 (1974).

[17] S. R. Langhoff and E. R. Davidson, Int. J. Quant. Chem., **8**, 61 (1974).

[18] T. Fueno and R. J. Buenker, Theor. Chim. Acta, **73**, 123 (1988).

[19] M. W. Chase, Jr., C. A. Davies, J. R. Downey, Jr., D. J. Frurip, R. A. McDonald, and A. N. Syverud, JANAF thermochemical Tables, 3rd ed. National Bureau of Standards, Washington, D. C. (1985).

[20] A. D. Walsh, J. Chem. Soc., 2266 (1953).

[21] M. J. S. Dewar, J. P. Ritchie, and J. Alster, J. Org. Chem., **50**, 1031 (1985).

[22] H. E. O'Neal and S. W. Benson, Kinetic Data on Gas Phase Unimolecular Reactions. NSRDS-NB521, Washington, D.C. (1970).

[23] A. M. Wodtke, E. J. Hintsa, and Y. T. Lee, J. Phys. Chem., **90**, 3549 (1986).

[24] M. L. McKee, J. Phys. Chem., **93**, 7365 (1989).

[25] R. P. Saxon and M. Yoshimine J. Phys. Chem., **93**, 3130 (1989).

Table 1. The reference configurations used in the CI calculations and their weights[a]

	Configurations	$\|C_i\|^2$
HNO_2 (**1**)		
	$\ldots(1b_1)^2(4b_2)^2(6a_1)^2(1a_2)^2$	0.8681
	$(1b_1)^2 \rightarrow (2b_1)^2$	0.0037
	$(1a_2)^2 \rightarrow (2b_1)^2$	0.0249
	$(1b_1) \rightarrow (2b_1)$	0.0039
TS		
	$\ldots(2a'')^2(10a')^2$	0.8722
	$(2a'')^2 \rightarrow (3a'')^2$	0.0144
	$(1a'')^2 \rightarrow (3a'')^2$	0.0042
	$(1a'') \rightarrow (3a'')$	0.0040
	$(2a'') \rightarrow (3a'')$ $(10a') \rightarrow (13a')$	0.0030
trans-HONO (**2**)		
	$\ldots(10a')^2(2a'')^2$	0.8878
	$(1a'')^2 \rightarrow (2a'')^2$	0.0076
	$(1a'')^2 \rightarrow (3a'')^2$	0.0039
	$(10a') \rightarrow (12a')$ $(2a'') \rightarrow (3a'')$	0.0036
	$(1a'') \rightarrow (3a'')$ $(2a'') \rightarrow (3a'')$	0.0035

a The MRD-CI calculations were carried out at the RHF SCF optimized geometries shown in Fig. 1(a).

Table 2. Comparisons of the vertical excitation energies ΔE_{CI}^{vert} of HNO_2, O_3 and SO_2

		ΔE_{CI}^{vert} (eV)		
		HNO_2 [a]	O_3 [b]	SO_2 [b]
$^1A_1$				
	1 (ground-state)	(0)	(0)	(0)
	2 (6π)	10.6	4.5	8.7
	3	10.5	6.7	9.0
$^1A_2$				
	1	4.8	2.2	4.9
	2	10.3	6.4	8.5
	3	12.0		
$^1B_1$				
	1	4.8	2.3	4.5
	2	11.4	7.2	8.3
	3	13.2		
$^1B_2$				
	1	7.5	5.1	6.7
	2	10.8	6.8	9.8
	3	12.3		

a At the CASSCF(8,6)/6-31G** optimized geometry of the ground-state HNO_2.

b At the MRD-CI optimized geometries [18].

Table 3. Calculated bond lengths (Å), angles (deg) and dihedral angles (deg) of the transition state for the isomerization HNO_2 → *trans*-HONO

	R(N-H)	R(N-O^3)	R(N-O^4)	∠O^3NH	∠O^4NO^3	<O^4NO^3H [b]
RHF/STO-3G	1.142	1.350	1.256	67.4	139.7	114.0
C_s restricted [a]	(1.130)	(1.348)	(1.247)	(64.9)	(127.7)	(180.0)
RHF/4-31G	1.189	1.330	1.175	62.3	125.8	180.0
RHF/6-31G**	1.152	1.268	1.162	62.9	124.8	180.0
CAS(8,6)/6-31G**	1.142	1.345	1.175	60.4	125.0	180.0

a RHF/STO-3G results for the case where the geometry is restricted to the planar (C_s) form. The geometry takes on two imaginary frequencies.

b Dihedral angles.

Table 4. Results of the SCF and MRD-CI calculations

	E_{SCF} + 204 (hartree)	ΔE_{CAS} (kJ/mol)	E_{CI} + 205 (hartree)	ΔE_{CI} (kJ/mol)	ΔE_0 [a] (kJ/mol)	$\Delta H°$ (kJ/mol)
$H + NO_2$	-0.52176[b]		-0.03822[c]	354	319	325
HNO_2 (**1**)	-0.62110	34	-0.14385	62	66	
TS	-0.51539	303	-0.07241	253	237	
trans-HONO (**2**)	-0.64401	(0)	-0.17263	(0)	(0)	(0)
NO + OH	-0.62582[b]		-0.09768[c]	198	175	201

a The subscript 0 stands for CI + vib.

b Sum of the UHF energies of the fragment radicals.

c The energies were calculated for the supermolecule models. See text.

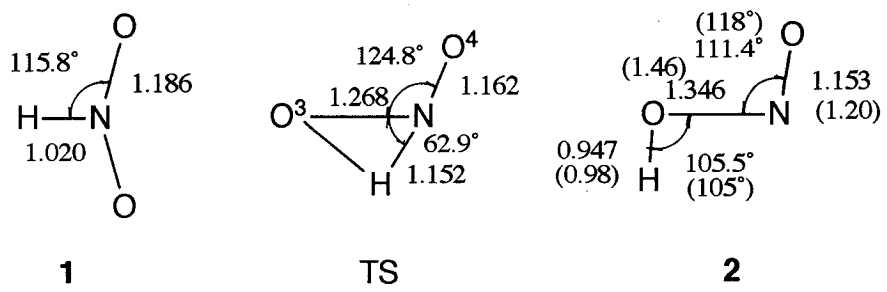

(a) RHF/6-31G** optimized geometries

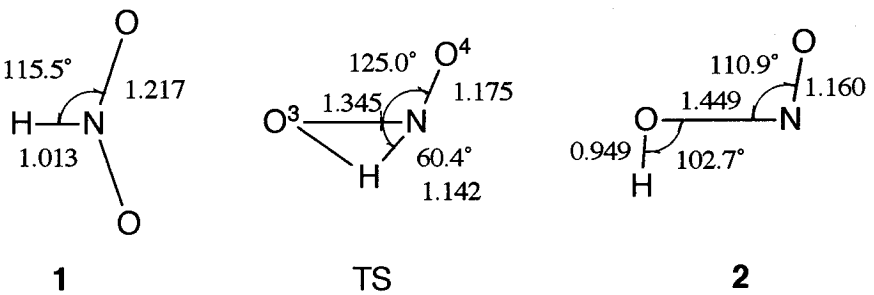

(b) CASSCF/6-31G** optimized geometries

Figure 1. Geometries of hydrogen nitryl (**1**), the transition state (TS) and trans-HONO (**2**) optimized by (a) the RHF/6-31G** and (b) the CASSCF/6-31G** procedure. The bond lengths are given in units of Å.

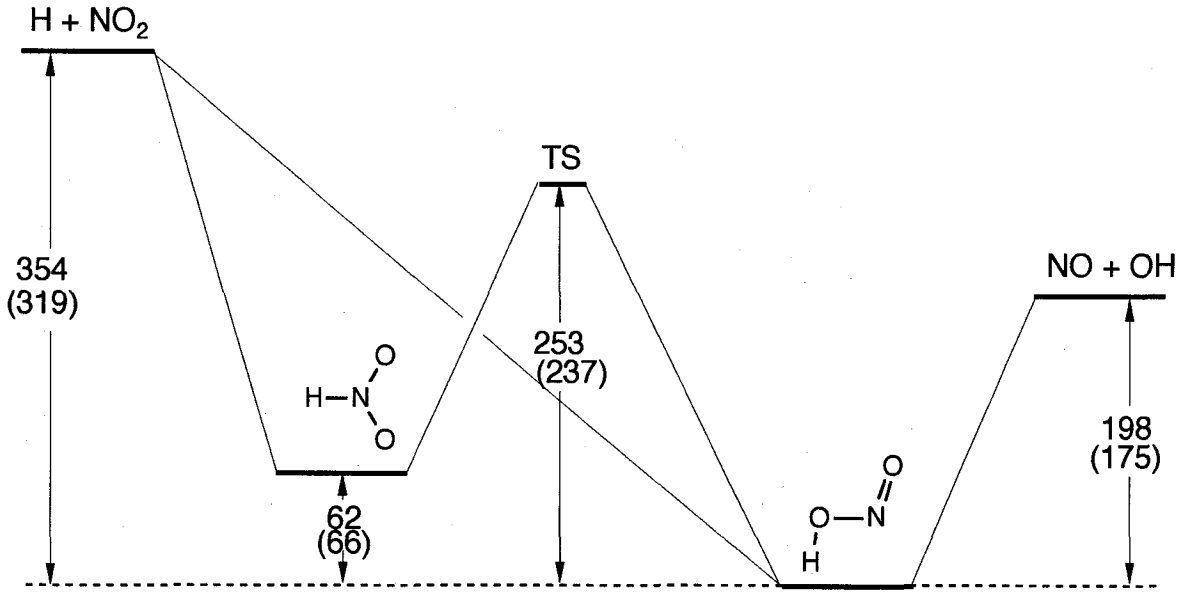

Figure 2. Potential energy profiles (ΔE_{CI}) calculated for the HNO_2 - HONO system. Energy gaps shown are in units of kJ/mol. Given in parentheses are the energy differences (ΔE_0) obtained with the vibrational zero-point energy corrections.

Chapter 3

Theoretical Study of the Rates and Mechanism of the Gas-Phase Reaction $H + HN_3 \rightarrow NH_2 + N_2$

Reaction of the hydrogen atom with hydrazoic acid HN_3 in the gas phase has been investigated theoretically. Tracing of the reaction path by the SCF procedure based on the 6-31G(*d*, *p*) basis functions has shown that the reaction proceeds through an initial rate-determining hydrogen atom addition to HN_3 giving a doublet radical H_2N_3 and its subsequent self-decomposition into $NH_2 + N_2$. The barrier height for the initial addition step calculated by the MRD-CI method employing the [4*s*2*p*1*d*] basis sets is 23 kJ/mol. The bimolecular rate constants for the overall reaction calculated by the conventional transition state theory combined with appropriate tunneling corrections are found to agree well with the experimental data reported over the temperature range 300 to 500 K.

1. Introduction

The bimolecular reaction of the hydrogen atom with hydrazoic acid HN_3 is known to be an unavoidable side reaction in the thermal decomposition of HN_3 [1]. It is so much so as the triplet imidogen radicals $NH(^3\Sigma^-)$ generated by the primary decomposition of HN_3 tend to be readily "self-recombined" to give N_2 +2H. HN_3 as the parent compound is much more susceptible to the attack of H than to $NH(^3\Sigma^-)$.

A direct kinetic study [2] of the reaction between H and HN_3 has shown that the product is exclusively NH_2:

$$H + HN_3 \longrightarrow NH_2 + N_2 \qquad (1)$$

Apparently, reaction (1) is far more advantageous than the abstraction reaction:

$$H + HN_3 \longrightarrow H_2 + N_3 \qquad (2)$$

The situations can be taken as indicating that the initial step of the H - HN_3 reaction will be an addition reaction

$$H + HN_3 \longrightarrow \underset{\mathbf{1}}{\overset{H}{\underset{H}{\diagdown\!\diagup}}\!\!N-NN} \qquad (3)$$

the doublet adduct thus formed being decomposed subsequently to $NH_2 + N_2$:

$$\mathbf{1} \longrightarrow NH_2 + N_2 \qquad (4)$$

Admitting that the reaction of our concern, reaction (1), is in reality a two-step reaction comprising reactions (3) and (4), we are required to answer several questions of importance. They include the following:

1. Can the adduct **1** be a well-definable intermediate?

2. Which of the two successive reactions, (3) and (4), is rate-determining? More specifically, which of the respective transition states will energetically be less stable?

3. Can the characteristics of the net transition state located be compatible with the experimentally determined rate constants [2]?

The present work is aimed at answering all these questions. To this end, we trace the reactions (3) and (4) by the SCF/6-31G(d, p) procedure. The stationary points located are then subjected to the MRD-CI computations using the [4s2p1d] basis functions. The bimolecular rate constants for the overall reaction (1) are calculated by the conventional transition state theory (TST) [3]. Kinetic features and mechanism of the reaction will be discussed in the light of the theoretical results obtained.

2. Method of calculations

The reaction paths were traced by the UHF SCF procedure combined with the energy gradient technique. The Gaussian 86 program package [4] was used for this purpose. The basis sets used are the 6-31G(d, p) functions [5] throughout. The validity of the geometries for the transition states located were checked by the vibrational analyses.

All the stationary points involved in the potential energy surface swept were then subjected to the multi-reference double-excitation (MRD) configuration-interaction (CI) computations. The Table MRD-CI formalism furnished by Buenker [6, 7] was used. The basis sets used for the CI computations were the conventional 6-31G(d, p) functions and the [4s2p]/[2s] functions due to Dunning [8] augmented with one set each of d or p polarization functions. In obtaining the CI energy, we followed the configuration-selection routine, extrapolation technique, and the Langhoff-Davidson perturbation corrections, as has been described in detail in our previous papers.[9-11] The maximal dimension of the present CI computations are ca. 15000 while the total

numbers of the symmetry-adapted configurational functions are ca. 800,000.

3. Results

3.1. Adduct Radical

The doublet radical H_2N_3 comprising of hydrazoic acid HN_3 and a hydrogen atom can either be an asymmetric adduct HHN_3 (**1**) or a symmetric entity HN_3H (**2**). SCF geometry optimizations of these radicals by use of the 6-31G(*d, p*) basis sets gave the structures as shown in Fig. 1. The former radical **1** has proved to be nonplanar, while the latter **2** is planar (C_{2v}) symmetric. In terms of the UHF SCF energies, **1** and **2** are more stable than the binary system H + HN_3 by 254 and 184 kJ/mol, respectively.

By separate computations, it has been confirmed that **1** is state-correlated with H + $HN_3(\tilde{X}^1A')$, whereas **2** with H + $HN_3(^3A'')$. The situation indicates that the addition of the hydrogen atom toward HN_3 in its ground state ($\tilde{X}^1A'$) should take place on the terminal nitrogen atom bearing the H atom exclusively. This, in turn, justifies the presumption that the initial step of the H - HN_3 reaction of our present concern will be reaction (3). In what follows, therefore, we will focus our attention on the behavior of the asymmetric radical HHN_3(**1**).

3.2. Potential Energy Profiles

To begin with, the transition state (TS1) of the initial H atom addition reaction (3) was located by the SCF/6-31G(*d, p*) procedure. The optimal geometry obtained for TS1 is shown in Fig. 2. Judging from the dihedral angles appended, it appears that the incoming hydrogen atom (H^5) starts to approach the N^1 atomic site from the direction perpendicular to the molecular plane of HN_3. The calculated SCF barrier height was 50 kJ/mol.

The subsequent decomposition process of **1**, reaction (4), was then traced by the SCF procedure in the attempt to locate its transition state (TS2). The SCF saddle point

showed up at the N^1-N^2 separation of 1.59 Å. The point was found to lie only 14 kJ/mol above **1** and to be 56 kJ/mol less stable than the $NH_2(^2A_1) + N_2$ system as the decomposition product. TS2 is thus far lower-lying than TS1 and is even more stable than the initial state $H + HN_3$. Clearly, the initial H atom addition step, reaction (3), is rate-determining for the overall reaction (1).

All the stationary points mentioned so far were subjected to the MRD-CI calculations using the 6-31G(*d, p*) and Dunning's [4*s*2*p*1*d*] basis functions. The CI energies obtained and the vibrational zero-point corrected data thereof (CI + vib), both expressed by taking the initial $H + HN_3$ system as reference, are summarized in Table 1. The UHF SCF energies are also included there for the sake of comparison. It should be mentioned here that, in evaluating the CI energy of TS2, a series of CI computations were carried out at several points on the SCF reaction path to locate the point of the CI maximum. The geometry of TS2 given in Fig. 2 corresponds, in reality, to such a point where the N^1-N^2 linkage (1.89 Å) has considerably been elongated as compared to that in the SCF saddle point and is now more than 100 kJ/mol less stable than the adduct radical **1**. The conclusion that TS2 is by far lower-lying than TS1 remains unaltered.

As can be seen in Table 1, the activation barrier heights for the rate-determining step (TS1) calculated by the MRD-CI/[4*s*2*p*1*d*] method, 19.9 (CI) and 22.7 (CI + vib) kJ/mol, are in reasonably good agreement with the experimental activation energy E_a = 19 kJ/mol [2]. Also, the heat of reaction calculated for the overall process (1) by the same basis set, -322 kJ/mol (CI + vib), agrees nearly perfectly with the experimental value of ΔH_0° = -320 kJ/mol [12].

Figure 3 is a diagrammatic illustration of the potential energy profiles for the H + HN_3 system calculated by the present MRD-CI/[4*s*2*p*1*d*]//6-31G(*d, p*) procedure. The energy gaps shown are all based on the CI energies with the vibrational zero-point energy corrections. That the reaction between H and HN_3 should end up with the formation of $NH_2(^2B) + N_2$ via the rate-controlling TS1 is self-explanatory.

3.3. Rate Constants

We are now in a position to calculate the bimolecular rate constants for reaction (**1**) according to the conventional transition state theory (TST). The vibrational frequencies calculated by the SCF/6-31G(*d*, *p*) procedure for the reactant HN_3 are 516.6, 609.3, 1130, 1292, 2260, and 3361 cm^{-1} (corrected by a constant factor of 0.90), which give the vibrational zero-point energy of 54.8 kJ/mol. The frequencies calculated by the same token for TS1 are 339.4, 454.0, 551.1, 635.2, 1058, 1286, 1942, and 3375 cm^{-1} with one additional imaginary frequency of $1130i$ cm^{-1}.

The rate constants k have first been calculated by adopting the [4*s*2*p*1*d*] theoretical activation energy E_0 = 23 kJ/mol over the temperature range 300-500 K. The results are indicated by dotted lines in Fig.4, where they are seen to be by a factor of 3 to 6 too low as compared with the experimental results [2], which are represented by the Arrhenius parameters $A = 1.53 \times 10^{13}$ $cm^3mol^{-1}s^{-1}$ and E_a = 19 kJ/mol. Apparently, the discrepancy is due partly to a possible overestimation of the E_0 value; the disagreement cannot be remedied unless E_0 is lowered artificially to ca. 19 kJ/mol.

It is our feeling that another factor of importance which needs to be taken into consideration is the tunneling effect operative in the region of TS1. For evaluating the tunneling correction factors Γ at various temperatures, we adopt here Johnston's method [14] based on the Eckart potential model. The detail of the method is described in chapter 1 of this thesis. Γ can generally be expressed as

$$\Gamma \equiv \frac{J}{J_c} = \frac{e^{V_1/RT}}{RT}\int_0^\infty \kappa(E)e^{-E/RT}dE \qquad (5)$$

where $\kappa(E)$ is the one-dimensional penetration probability through the barrier at a given internal energy E. $\kappa(E)$ is a function of the Eckart potential parameters V_1, V_2, and F^*, where V_1 and V_2 denote the heights of the barrier top above the reatant and product potential-energy minima, respectively, and where F^* is the second derivative of the potential energy function at the barrier top. In the present instance, $V_1 = E_0$ and $V_2 = E_0$

+ 180 kJ/mol. F^* is related to the imaginary frequency $\nu^{\ddagger}$ of the vibrational normal mode responsible to the motion of the hydrogen atom at TS1; specifically, $\nu^{\ddagger} = 1130i$ cm^{-1} in the present case.

The Γ values at various temperatures were calculated according to eq. (5) by numerical integration on a computer. The rate constants k calculated by multifying these Γ values at the temperature range 300-500 K are shown by full lines in Fig. 4. Use of the theoretically obtained activation energy E_0 = 23 kJ/mol is still incapable of reproducing the experimental curve sufficiently well. The best fit of the calculated results with experiments is reached by adopting E_0 = 21 kJ/mol. Yet, this much of fluctuation of the E_0 value will be admissible.

4. Discussion

As has already been described above, both the activation energy and the exoergicity of the entire reaction (1) are reproduced reasonably well by the present CI computations based on the [4*s*2*p*1*d*] basis functions. In view of this success, calculations of other energies related to the adduct radical (**1**) will also be sufficiently reliable. Thus, the H-N bond dissociation energy of **1** is calculated to be 365 kJ/mol, a value which is somewhat smaller than 440 kJ/mol for NH_3. The energy barrier of **1** against its decomposition into $NH_2 + N_2$ is predicted to be 144 kJ/mol. It seems, therefore, that the doublet radical **1** is a fairly stable entity and could well be identified as such when the H atom addition toward HN_3 is conducted under high pressures at low temperatures.

Also shown in Fig. 3 is the energy level for the planar ($^2A'$) form of HHN_3, which corresponds to the transition state for the "umbrella inversion" of HHN_3. The calculated inversion energy is 103 kJ/mol, which is significantly greater than the experimental value of 24 kJ/mol for the case of NH_3.

At this stage, we would like to point our one feature of importance regarding the discomposition process (4). We have noticed that, as the N^1-N^2 bond of **1** is elongated,

its NH_2 moiety is rotated increasingly around the N^1-N^2 axis until it attains a C_s-symmetric form at TS2. Beyond TS2, the entire system maintains the C_s symmetry all the way. A dynamical consequence of this computational feature is that the NH_2 radical at the instance of its formation by the decomposition should be rotationally excited.

Finally, we will comment briefly on the abstraction reaction (2), which has been left out of account at the onset. Geometry optimization of the transition state (TS3) by the UHF/SCF procedure has given a structure as shown in Fig. 5. Results of the subsequent MRD-CI calculations are listed in the final line of Table 1. The activation energy (CI + vib) obtained by the use of the [4*s*2*p*1*d*] basis functions is 47 kJ/mol, which is clearly greater than that (23 kJ/mol) calculated for the addition reaction (**1**). Accordingly, the possibility of the abstraction reaction participating in the H-HN_3 reaction must be less than 0.5 % in the temperature region of our interest. Ignoring the role of the abstraction reaction in the H-HN_3 reaction is thus most likely to be legitimate.

5. Conclusions

1. The gas-phase reaction $H + HN_3 \longrightarrow NH_2 + N_2$ should proceed through the rate-determining addition of H toward HN_3, the calculated barrier height being 23 kJ/mol.

2. The adduct radical HHN_3 could be a well-definable entity, which is , however, readily be collapsed into $NH_2 + N_2$.

3. The conventional transition-state theory is capable of reproducing the bimolecular rate constants for the entire reaction in the temperature region 300-500 K.

References

[1] O. Kajimoto, T. Yamamoto, and T. Fueno, J. Phys. Chem., **83**, 429 (1979).

[2] G. Le Bras and J. Combourieu, Int. J. Chem. Kinet., **5**, 559 (1973).

[3] S. Glastone, K. J. Laidler, and H. Eyring, *The Theory of Rate Processes*, Mc-Graw-Hill, New York (1941).

[4] M. J. Frisch, J. S. Binkley, H. B. Schlegel, K. Raghavachari, C. F. Melius, R. L. Martin, J. J. P. Stewart, F. W. Bobrowicz, C. M. Rohlfing, L. R. Kahn, D. J. DeFrees, R. Seeger, R. A. Whiteside, D. J. Fox, E. M. Fleuder, S. Topiol, and J. A. Pople, GAUSSIAN 86, Carnegie-Mellon Quantum Chemistry Publishing Unit. Pittsburgh (1984); IMS version registered by N. Koga, S. Yabushita, K. Sawabe, and K. Morokuma.

[5] W. J. Hehre, R. Ditchfield, and J. A. Pople, J. Chem. Phys., **56**, 2257 (1972); P. C. Hariharan and J. A. Pople, Theor. Chim. Acta (Berl.), **28**, 213 (1973).

[6] R. J. Buenker, *Studies in Physical and Theoretical Chemistry*, vol. 21, ed. by R. Carbo, Elsevier, Amsterdam, pp17-34 (1982).

[7] R. J. Buenker and R. A. Phillips, J. Mol. Struct. (Theochem), **123**, 291 (1985).

[8] T. H. Dunning, Jr., J. Chem. Phys., **53**, 2823 (1970).

[9] T. Fueno, K. Yamaguchi, and O. Kondo, Bull. Chem. Soc. Jpn., **63**, 901 (1990).

[10] K. Yokoyama, S. Takane, and T. Fueno, Bull. Chem. Soc. Jpn., **64**, 2230 (1991).

[11] T. Fueno, K. Yokoyama, and S. Takane, Theor. Chim. Acta (Berl.), **82**, 299 (1992).

[12] S. W. Benson, *Thermochemical Kinetics*, 2nd ed., Wiley, New York (1976).

[13] G. Herzberg, *Electronic Spectra and Electronic Structure of Polyatomic Molecules*, D. van Nostrand Co., New York (1966).

[14] H. S. Johnston, *Gas Phase Reaction Rate Theory*, Ronald Press, New York (1966), pp. 40-47.

Table 1. Relative MRD-CI energies (kJ/mol) of the H-HN_3 system calculated by use of the 6-31G(*d*, *p*) and [4*s*2*p*1*d*] basis functions

State	6-31G(*d*, *p*)			[4*s*2*p*1*d*]		Expt.
	UHF SCF	CI	CI + vib	CI	CI + vib	
$H + HN_3$	(0)[a]	(0)[b]	(0)[b]	(0)[c]	(0)[c]	(0)
TS1	49.5	26.7	29.6	19.9	22.7	19[d]
HHN_3 (**1**)	-254	-347	-319	-392	-365	
HHN_3 ($^2A'$)	-243	-266	-242	-287	-262	
HN_3H (**2**)	-184	-13	12	-32	-7	
TS2	-240	-230	-219	-232	-221	
$NH_2(^2B_1) + N_2$	-437	-321	-309	-334	-322	-320[e]
$NH\ (^2A_1) + N_2$	-296	-182	-169	-193	-180	-198[f]
TS3	78	78	69	56	47	

a E_{SCF} = -164.34113 hartrees.

b E_{CI} = -164.86271 hartrees; E_{vib} = 54.8 kJ/mol.

c E_{CI} = -164.89448 hartrees; E_{vib} = 54.8 kJ/mol.

d Experimental activation energy, E_a .[2]

e Based on the thermochemical data, ΔH°_0. [12]

f The excitation energy (123 kJ/mol) [13] was corrected for the vibrational zero-point energy.

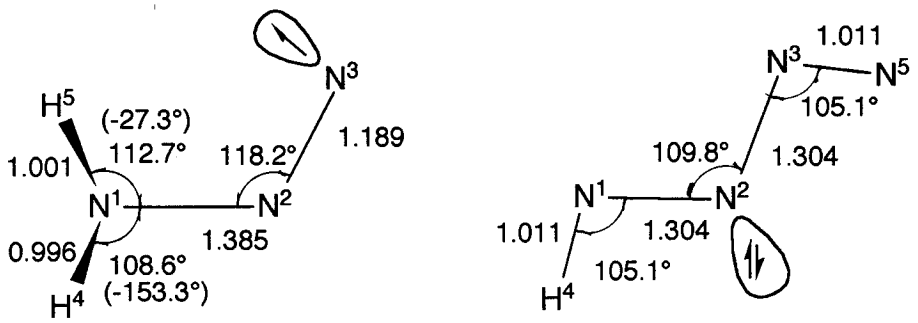

HHN_3 HN_3H ($^2A_2$)

Figure 1. Optimized geometries of HHN_3 (**1**) and HN_3H (**2**). The bond lengths are given in units of Å. The entries given in parentheses indicate the dihedral angles ϕ(HNNN).

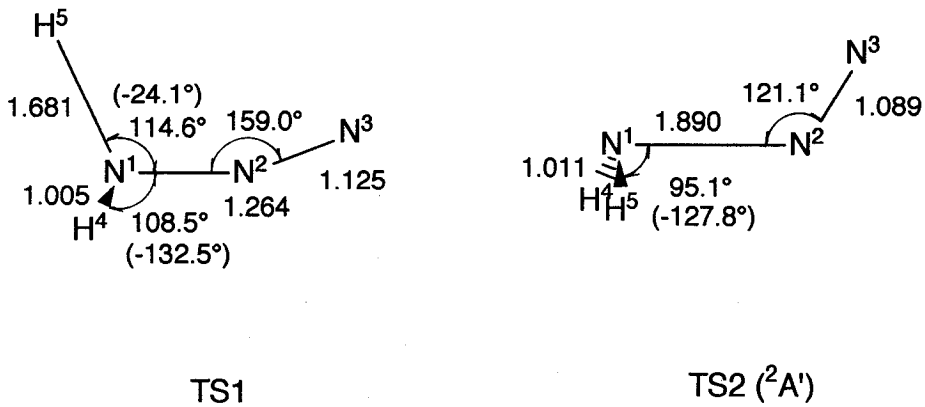

Figure 2. Optimized geometries of the transition states. The bond lengths are given in units of Å. The entries given in parentheses indicate the dihedral angles ϕ(HNNN). TS1, reaction (3); TS2, reaction (4)

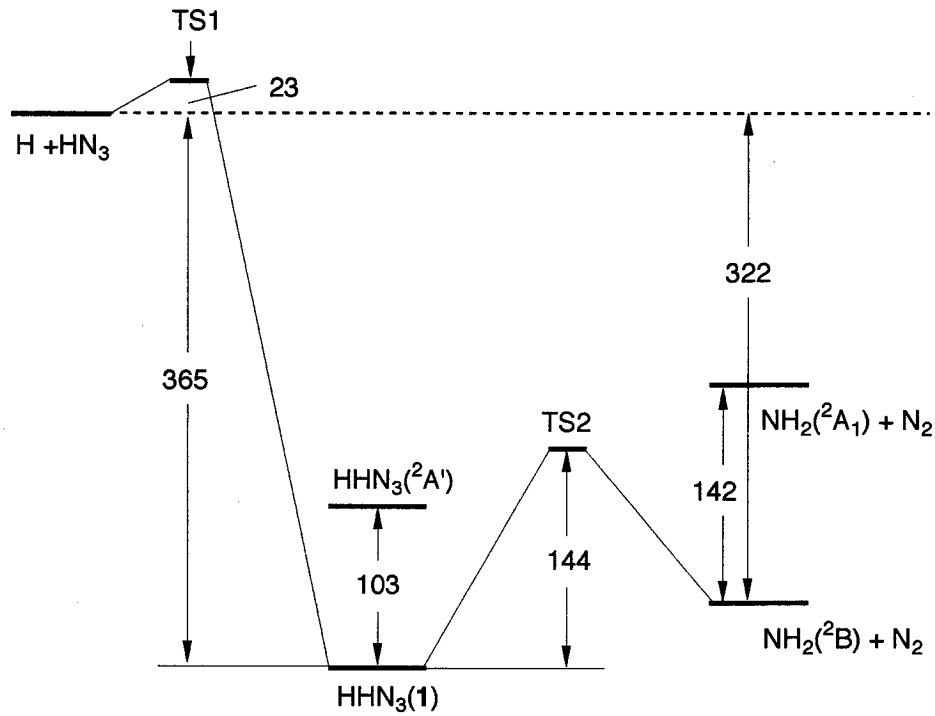

Figure 3. Potential energy profiles of the H-HN_3 system calculated by the MRD-CI method employing the [4*s*2*p*1*d*] basis functions. Energy gaps shown are in units of kJ/mol.

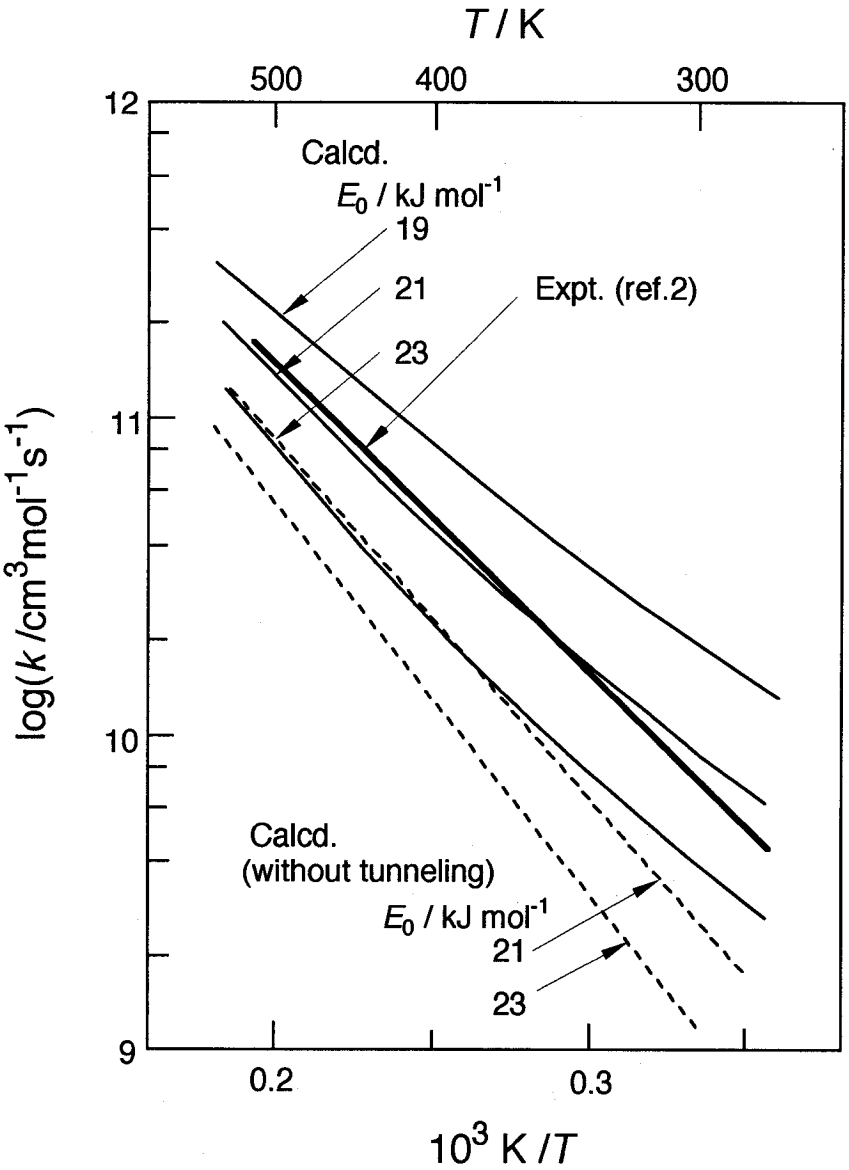

Figure 4. Rate constants for the gas-phase reaction H + HN_3 → NH_2 + H_2. *Broken lines*, calculated by the conventional TST without the tunneling correction; *full lines*, calculated by the TST formalism with the tunneling corrections; *bold line*, experimental results reported by G. Le Bras and J. Combourieu [2].

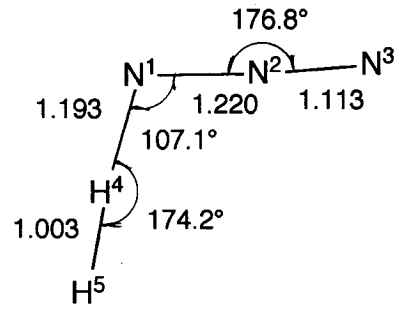

TS3 (^{2}A')

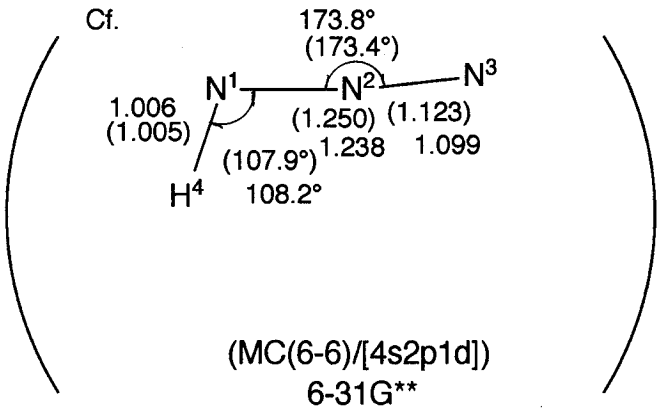

(MC(6-6)/[4s2p1d])
6-31G**

Figure 5. Optimized geometry of the transition state for the abstraction reaction $H + HN_3 \rightarrow H_2 + N_3$. The bond lengths are given in units of Å.

Chapter 4

Ab Initio CI Study of the Hydrogen Abstraction Reactions of NH($^1\Delta$) from Methane and Ethane

Potential energy profiles for the hydrogen atom abstraction reactions of the NH($^1\Delta$) diradical from methane and ethane have been investigated by ab initio molecular orbital computations using the 6-31G(*d*) and 6-31G(*d*, *p*) basis functions. The reactions are found to proceed by maintaining the C_s symmetry. To locate the transition states, multi-reference double-excitation (MRD) CI calculations were carried out at several path points on the reaction paths traced by the SCF geometry optimization procedure. The activation barrier heights obtained for the reactions with methane and ethane are 53 and 38 kJ/mol, respectively, which are reduced respectively to 45 and ca. 25 kJ/mol upon the vibrational zero-point energy corrections. The relatively low barrier heights are compatible with the efficiency of the hydrogen abstraction reaction of NH($^1\Delta$) observed in the gas phase.

1. Introduction

In a series of experimental work [1], we have gained clear-cut evidence that the singlet imino radical NH($^1\Delta$) can directly abstract a hydrogen atom from paraffins in the gas phase.

$$NH(^1\Delta) + RH \longrightarrow NH_2 + R \qquad (1)$$

The most salient feature of the reaction is that it proceeds in a manner of competition with the insertion reaction giving amines as the more efficient pattern of elementary reactions. Since the insertion reaction is a nearly collision-controlled (i.e., essentially no-activation-barrier) process [2], the abstraction reaction must inherently be an elementary process of relatively low activation energy.

Theoretically, the radical character of NH($^1\Delta$) is a consequence of the duality of its electronic structure due to the presence of the degenerate valence orbitals. Adopting the conventional Cartesian-coordinate orbitals, p_x and p_y, the angular part of NH($^1\Delta$) can be expressed in two distinct forms; (a) a two-configurational closed-shell ^{1}A' representation $[(p_x)^2 - (p_y)^2]/\sqrt{2}$ and (b) a single-configurational open-shell ^{1}A" representation $(p_x)(p_y)$ [2, 3]. Apparently, it is the latter diradical (^{1}A") structure that is responsible for the abstraction reaction, while the former (^{1}A') structure permits NH($^1\Delta$) to be an electrophile favoring the insertion reaction.

The role of the open-shell character of NH($^1\Delta$) in the hydrogen abstraction reaction has been demonstrated theoretically, in a preliminary communication, for the case of molecular hydrogen [4]. It was shown that the reaction proceeds by maintaining the planar (^{1}A") symmetry. The activation barrier height calculated by the multi-reference double-excitation (MRD) CI method employing the conventional 4-31G basis functions was no greater than 38 kJ/mol.

The present work is an extension of the above-mentioned preliminary investigation

[4] to the cases of methane and ethane. In both cases, the minimum-energy paths of abstraction were traced by the open-shell Hartree-Fock SCF procedure, using the 6-31G(*d*, *p*) basis functions. MRD-CI calculations were then carried out at several points on the SCF reaction paths, to locate the transition states (TS). It will be shown that the effects of electron correlation are enormously large in the region of TS. The barrier heights obtained are 45 and 25 kJ/mol for the cases of methane and ethane, respectively, which are low enough to permit the reactions to proceed thermally in the room temperature region. The heats of reaction calculated have also proved to agree well with the experimental thermochemical data.

2. Method of calculations

$NH(^1\Delta)$ undergoing the hydrogen atom abstraction from RH (R = alkyl) can be regarded as a singlet diradical, which is most adequately represented by an open-shell $^1A''$ configuration. As a consequence, the reacting systems are expected to follow the paths conforming to the $^1A''$ representation as well. In addition, adequate descriptions of the systems along the reaction paths must entail reliable assessment of the electron correlation effects. Thus, our tactics here is to trace the reaction paths by an open-shell SCF procedure and to conduct accurate CI calculations at several path points. The ultimate purpose is to locate and characterize the transition state on the basis of reliable CI calculations.

The paraffin molecules treated in this work are methane (R = CH_3) and ethane (R = C_2H_5). In tracing the reaction paths, the unrestricted Hartree-Fock (UHF) SCF procedure was adopted, employing the 6-31G(*d*, *p*) basis functions [5]. The exponents used for the *d* and *p* functions are 0.8 and 1.1, respectively. For the sake of comparison, similar reactions of $NH(^3\Sigma^-)$ have also been treated. The Gaussian 86 program package

[6] was used for SCF geometry optimizations.

For CI calculations, the Table MRD-CI program furnished by Buenker [7, 8] was used. The configuration-selection and extrapolation routines [7] were followed. Thus, the minimum threshold T_m for the configuration selection was set to be a certain value between 5 to 20 μhartrees in order to select 8000-10000 symmetry-adopted configurational functions (SAF) out of the total SAF's generated. Additional threshold values T increasing stepwise from T_m at a 5-μhartrees interval were adopted to enable the extrapolation of the CI energy to the limit $T \rightarrow 0$. The limiting CI energy thus extrapolated will be denoted as $E_{CI,T\rightarrow 0}$.

In calculating the CI energies at a given set of T_m and T's, all the configurations whose contributions $|C_i|^2$ to a state under consideration exceeded 0.2 % were regarded as the reference (main) configurations. The total number of the reference configurations adopted were typically 1 to 5 depending on the size of the systems treated, and the total sum of the weights $|C_i|^2$ of the reference configurations ranged from 0.90 to 0.95.

The $E_{CI,T\rightarrow 0}$ values were further subjected to the generalized Langhoff-Davidson correction [9, 10]. The CI energy with this correction can be regarded as an estimate of the full CI limit value [10, 11]. Because this corrected CI energy is relatively insensitive to the number of the reference configurations chosen, we will adopt it as the final CI energy and will denote it as E_{CI}.

3. Results

3.1. Methane

First of all, the path of hydrogen abstraction by NH($^3\Sigma^-$) was traced by the UHF SCF procedure using the 6-31G(*d*)basis functions. The reaction has proved to proceed by maintaining the planar symmetric (C_s) structure of the entire reacting system. Geometry of the transition state (^{3}A") located is illustrated in Figure 1-(a). The

activation barrier height obtained was $\Delta E^{\ddagger}$= 176 kJ/mol. It has been confirmed that the transition state (TS) geometry provides one single imaginary frequency of vibration; ν^* = 2682i cm^{-1}.

The initial and final states of reaction as well as the transition state were then subjected to the MRD-CI calculations, using the 6-31G(d) and 6-31G(d, p) basis functions. The results of calculations are summarized in Table 1. It can be seen in Table 1 that the reaction is basically endothermic. The endothermicities (CI + vib) calculated by use of the 6-31G(d) and 6-31G(d, p) basis sets are ΔE = 72 and 68 kJ/mol, respectively. Apparently, the latter is in slightly better agreement with the experimental heat of reaction, ΔH_o° = 59 ± 13 kJ/mol [12, 13]. The activation energies (CI + vib) calculated with the two basis sets are ΔE = 140 and 141 kJ/mol, respectively, which do not differ appreciably.

In the case of reaction of NH($^1\Delta$), the reaction path was followed by the conventional singlet UHF SCF procedure. However, the UHF SCF descriptions of singlet diradical entities are theoretically no justifiable practice. Therefore, we have undertaken to conduct MRD-CI calculations at various points on the SCF reaction path to locate the TS. The results of CI calculations carried out by use of the 6-31G(d) basis set are shown in Figure 2, together with those for the triplet case. For both the cases, the difference in bond lengths, r(C-H)-R(H-N), has been chosen as the ordinate for the potential energy profiles. The geometry corresponding to the CI-energy maximum is regarded as the TS. The CI-based TS geometry for the singlet case is illustrated in Figure 1-(b). As can be seen in Figures 1 and 2, the reaction of NH($^1\Delta$) reaches TS at a somewhat earlier stage of reaction than does NH($^3\Sigma^-$).

The barrier height, $\Delta E^{\ddagger}$, and the energy change of reaction, ΔE, calculated for the abstraction reaction by NH($^1\Delta$) are given in Table 1. The reaction should be exothermic. The exothermicities (CI + vib) calculated by use of the 6-31G(d) and 6-31G(d, p), -107 and -110 kJ/mol, respectively, are found to agree reasonably well with the experimental heat of reaction, ΔH_0° = -92 ± 13 kJ/mol. The activation energies

(CI + vib) calculated using the latter basis set, $\Delta E^{\ddagger}$ = 45 kJ/mol, is clearly lower than the value, 53 kJ/mol calculated by use of the former set.

3.2. Ethane

The reactions of ethane with NH, both singlet and triplet, were treated likewise. Geometries for the transition states for the singlet (^{1}A") and triplet (^{3}A") reactions are as shown in Figure 3. The basis functions used are the 6-31G(*d*) sets. As in the case of methane, the ^{3}A" geometry is that of the UHF SCF saddle point, while the ^{1}A" geometry corresponds to the point of the maximum CI energy on the singlet UHF SCF minimum-energy path. Here also, the reaction of NH($^1\Delta$) is seen to reach TS somewhat earlier as compared to the reaction of NH($^3\Sigma^-$).

The results of MRD-CI calculations carried out by use of the 6-31G(*d*) basis sets at the TS geometries shown in Figure 3 are listed in the upper half of Table 2. The energy changes of reaction ΔE (CI + vib) calculated for the triplet and singlet cases are 60 and -119 kJ/mol, respectively. The former value is by 9-35 kJ/mol too large compared to the experimental heat of reaction, ΔH_0° = 38 ± 13 kJ/mol, whereas the latter is in good agreement with the experimental value of ΔH_0° = 117 ± 13 kJ/mol. The activation energies (CI + vib) are calculated to be 137 and 29 kJ/mol for the triplet and singlet reactions, respectively. Both these energies are evidently lower than the corresponding energies obtained for the reactions of CH_4 (Table 1).

MRD-CI calculations with the 6-31G(*d, p*) basis sets were practicable only for the initial and final states of reactions; the TS structures were too large in size to be handled at our present level of computational facilities. The energy change of reaction ΔE (CI + vib) calculated with the 6-31G(*d, p*) set are 54 and -123 kJ/mol, respectively, for the reactions of triplet and singlet NH. Apparently, the former value is an improvement over the 6-31G(*d*) value of 60 kJ/mol, while for the the reaction of NH($^1\Delta$) the effect of the hydrogen polarization functions is immaterial just as in the case of CH_4 (Table 1).

As for the activation energy (CI + vib) at the MRD-CI/6-31G(*d, p*) level of

sophistication, we can only make a guess at the stage of the present work. Judging from the differences in $\Delta E^{\ddagger}$ between the 6-31G(*d*) and 6-31G(*d, p*) calculation results for the case of CH_4 (Table 1), the $\Delta E^{\ddagger}$ in question for the reaction of C_2H_6 with $NH(^3\Sigma^-)$ would not alter largely from the 6-31G(*d*) result. $\Delta E^{\ddagger}$ for the reaction of $NH(^1\Delta)$, on the other hand, would probably be lowered by 4 kJ/mol or so, resulting thus in ca.25 kJ/mol.

4. Discussion

Major conclusions reached in this study are that the direct hydrogen abstractions of $NH(^1\Delta)$ from CH_4 and C_2H_6 are elementary reactions having relatively low activation energies. The activation energies $\Delta E^{\ddagger}$(CI + vib) calculated by employing the 6-31G(*d*) basis sets are 53 and 29 kJ/mol, respectively. By the use of 6-31G(*d, p*) function, these energies are likely to be reduced respectively to ca. 46 and 25 kJ/mol. Judging from the reasonably good agreements of the calculated heats of reaction ΔE(CI +vib) with the experimental data, -92 ± 13 and -117 ± 13, respectively, the above mentioned $\Delta E^{\ddagger}$/6-31G(*d, p*) values will be reliable enough. The greater exothermicity and the corespondingly lower activation energy for the reaction of C_2H_6 as compared to the case of CH_4 are simply a reflection of the lesser C-H bond dissociation energy for the former than for the latter, 410 and 435 kJ/mol, respectively [12, 13].

By the same token, it is to be expected that the activation energies for the reactions of C_3H_8 and iso-C_4H_{10} at the secondary and tertiary C-H bond positions will further be reduced in this order. The situation will permit their abstraction reactions to be competitive with the insertion reactions to the greater extents, in harmony with observations [1c].

Strictly speaking, however, the insertion reactions $NH(^1\Delta)$ into the C-H bonds of alkanes have to be looked into theoretically. Preliminary calculations have shown that, in the cases of CH_4 and C_2H_6, the activation barrier heights for the insertion are lower by ca. 25 and 13 kJ/mol, respectively, than those for the abstraction. Although there are

no calculation results for C_3H_8 and iso-C_4H_{10} at hand, the above delineated trends regarding the abstraction/insertion competitions will be most likely correct at least qualitatively.

5. Conclusions

(1) The hydrogen abstraction of NH($^1\Delta$) from alkanes is an elementary reaction, which proceeds by maintaining the planar symmetric ($^1A''$) structure of the entire reaction system.

(2) The exothermicities calculated by the MRD-CI/6-31G(*d*, *p*) procedure for the reactions of NH($^3\Sigma^-$) and NH($^1\Delta$) with CH_4 and C_2H_6 are in good agreement with the experimental heats of reactions.

(3) The activation energy obtained by the MRD-CI/6-31G(*d*) procedure for the abstraction reaction NH($^1\Delta$) + C_2H_6 ⟶ $NH_2 + C_2H_5$ is 29 kJ/mol, which is low enough to let the reaction compete with the more favorable insertion reaction NH($^1\Delta$) + C_2H_6 ⟶ $C_2H_5NH_2$. The results corroborate, though qualitatively, the conclusion reached from experimental work.

References

[1] (a) O. Kajimoto and T. Fueno, Chem. Phys. Lett., **80**, 484 (1981); (b) O. Kondo, J. Miyata, O. Kajimoto, and T. Fueno, Chem. Phys. Lett., **88**, 424 (1982); (c) O. Kondo, J. Miyata, S. Takane, and T. Fueno, to be publised.

[2] T. Fueno, V. Bonacic-Koutecky, J. Koutecky, J. Am. Chem. Soc, **105**, 5547 (1983).

[3] T. Fueno, J. Mol. Struct. (Theochem), **170**, 143 (1988).

[4] T. Fueno, O. Kajimoto, and V. Bonacic-Koutecky, J. Am. Chem. Soc., **106**, 406 (1984).

[5] P. C. Hariharan and J. A. Pople, Theor. Chim. Acta (Berl.), **28**, 213 (1973).

[6] M. J. Frisch, J. S. Binkley, H. B. Schlegel, K. Raghavachari, C. F. Melius, R. L. Martin, J. J. P. Stewart, F. W. Bobrowicz, C. M. Rohlfing, L. R. Kahn, D. J. DeFrees, R. Seeger, R. A. Whiteside, D. J. Fox, E. M. Fleuder, S. Topiol, and J. A. Pople, GAUSSIAN 86, Carnegie-Mellon Quantum Chemistry Publishing Unit. Pittsburgh (1984); IMS version registered by N. Koga, S. Yabushita, K. Sawabe, and K. Morokuma.

[7] R. J. Buenker, *Studies in Physical and Theoretical Chemistry*, ed. by R. Carbo, Elesevier, Amsterdam, Vol. 21, pp.17-34 (1982).

[8] R. J. Buenker and R. A. Phillips, J. Mol. Struct. (Theochem), **123**, 291 (1985).

[9] S. R. Langhoff and E. R. Davidson, Int. J. Quantum Chem., **8**, 61 (1974).

[10] P. J. Bruna and S. D. Peyerimhoff, *Ab initio Methods in Quantum Chemistry*, ed. by K. P. Lawley, Wiley-Interscience, New York, Part 1, pp.1-97 (1987).

[11] R. J. Buenker,. Int. J. Quantum Chem., **29**, 435 (1986).

[12] S. W. Benson, *Thermochemical Kinetics*, 2nd ed., Wiley, New York (1976).

[13] The experimental heat of formation, $\Delta H^{\circ}_{f0} = 3.65 \pm 0.10$ eV for $NH(^3\Sigma^-)$ has been taken from L. G. Piper, J. Chem. Phys. , **52**, 1303 (1982).

Table 1. Results of the MRD-CI calculations for the hydrogen abstraction reactions,

$NH + CH_4 \longrightarrow NH_2 + CH_3$

	$NH(^3\Sigma^-) + CH_4 \rightarrow NH_2 + CH_3$			$NH(^1\Delta) + CH_4 \rightarrow NH_2 + CH_3$		
	$E + 95$ [a] (hartree)	$\Delta E^{\ddagger}$ (kJ/mol)	ΔE (kJ/mol)	$E + 95$ [a] (hartree)	$\Delta E^{\ddagger}$ (kJ/mol)	ΔE (kJ/mol)
6-31G(*d*)//CI/6-31G(*d*)						
UHF SCF	-0.15459	176	102	-0.12122	123	-15
ROHF SCF	-0.14736	208	104	-0.07863	118	-77
CI, $T \rightarrow 0$	-0.41583	179	82	-0.34971	94	-92
CI	-0.42912	148	82	-0.36116	61	-96
CI + vib		140	72		53	-107
6-31G(*d, p*)//CI/6-31G(*d, p*)						
UHF SCF	-0.16435	169	92	-0.13128	117	5
ROHF SCF	-0.15726	199	96	-0.08895	112	-83
CI, $T \rightarrow 0$	-0.45775	176	78	-0.39171	85	-95
CI	-0.47311	149	79	-0.40546	53	-99
CI + vib		141	68		45	-110
Expt						
ΔH_0° [b]			59±13			-92±13

a For the initial state of reaction.

b Based on the experimental thermochemical data [12, 13].

Table 2. Results of the MRD-CI calculations for the hydrogen abstraction reactions, $NH + C_2H_6 \longrightarrow NH_2 + C_2H_5$

	$NH(^3\Sigma^-)+C_2H_6 \rightarrow NH_2+C_2H_5$			$NH(^1\Delta)+C_2H_6 \rightarrow NH_2+C_2H_5$		
	E + 134 [a] (hartree)	$\Delta E^{\ddagger}$ (kJ/mol)	ΔE (kJ/mol)	E + 134 [a] (hartree)	$\Delta E^{\ddagger}$ (kJ/mol)	ΔE (kJ/mol)
6-31G(*d*)//CI/6-31G(*d*)						
UHF SCF	-0.18817	167	89	-0.15480	115	0.8
ROHF SCF	-0.18094	198	92	-0.11221	110	-88
CI, $T \rightarrow 0$	-0.57187	199	65	-0.50575	63	-107
CI	-0.60103	146	71	-0.53307	38	-108
CI + vib		137	60		29	-119
6-31G(*d, p*)//CI/6-31G(*d, p*)						
UHF SCF	-0.19765	151	72	-0.16458	101	-15
ROHF SCF	-0.19056	182	76	-0.12225	97	-103
CI, $T \rightarrow 0$	-0.62499		56	-0.55895		-117
CI	-0.65875		65	-0.59110		-113
CI + vib		138 [c]	54		25 [c]	-123
Expt						
ΔH_0° [b]			38±13			-117±13

a For the initial state of reaction.

b Based on the experimental thermochemical data [12, 13].

c Estimated values (see text).

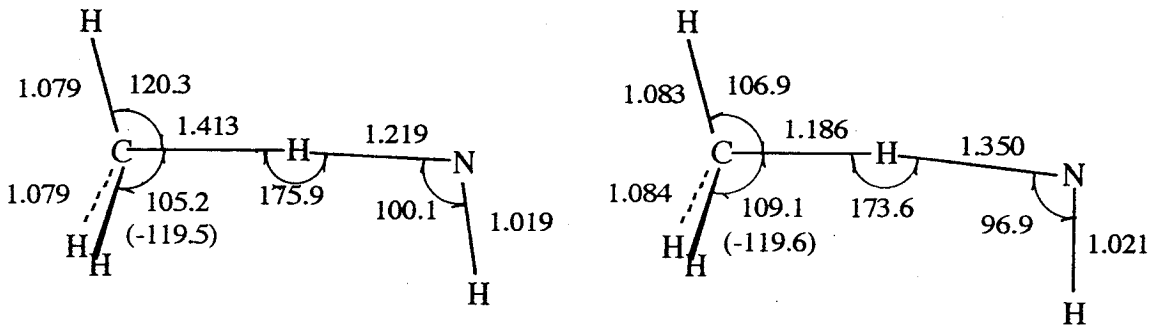

Figure 1. Geometries optimized for the transition states of the hydrogen abstractions of NH($^3\Sigma^-$) and NH($^1\Delta$) from CH_4. The basis sets used are the 6-31G(d) functions.

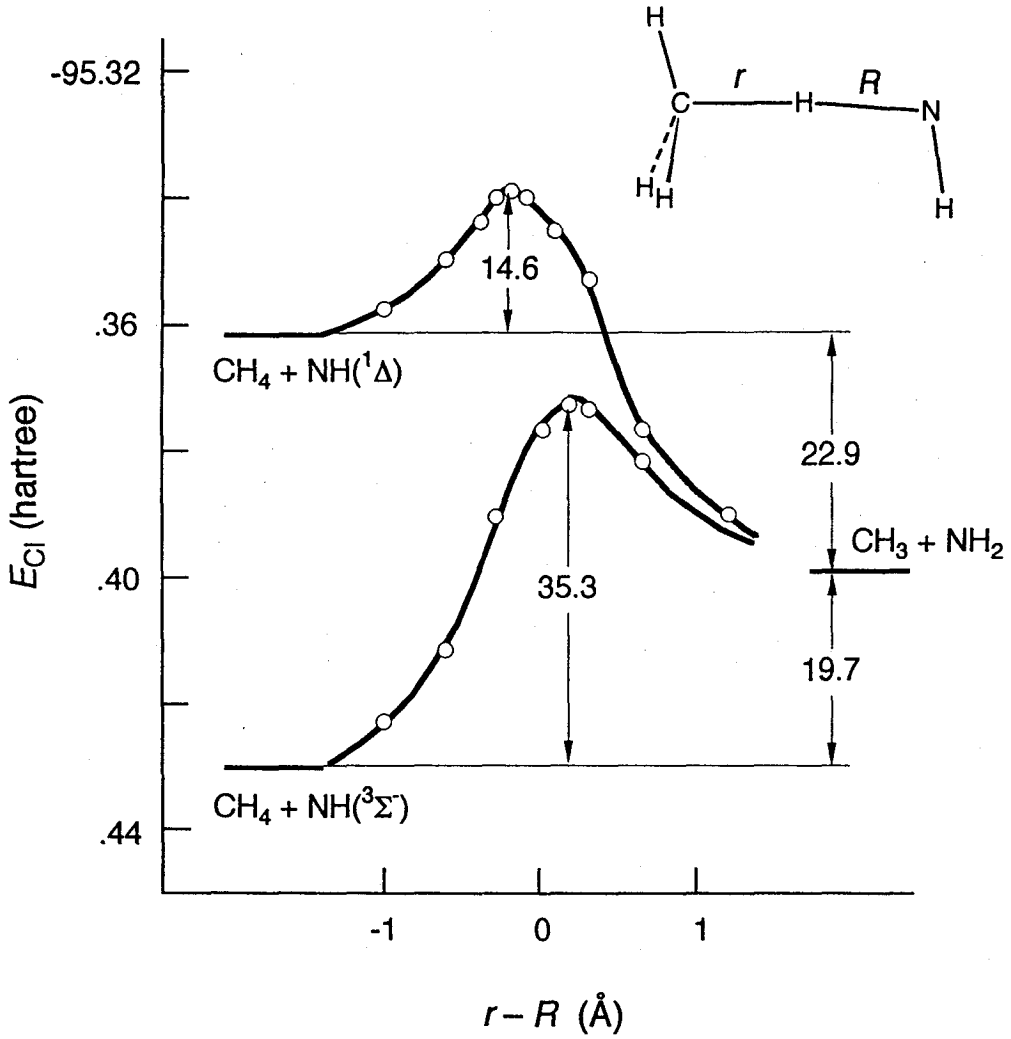

Figure 2. Potential energy profiles of the hydrogen abstractions of $NH(^3\Sigma^-)$ and $NH(^1\Delta)$ from CH_4 calculated by the MRD-CI procedure using the 6-31G(d) basis sets.

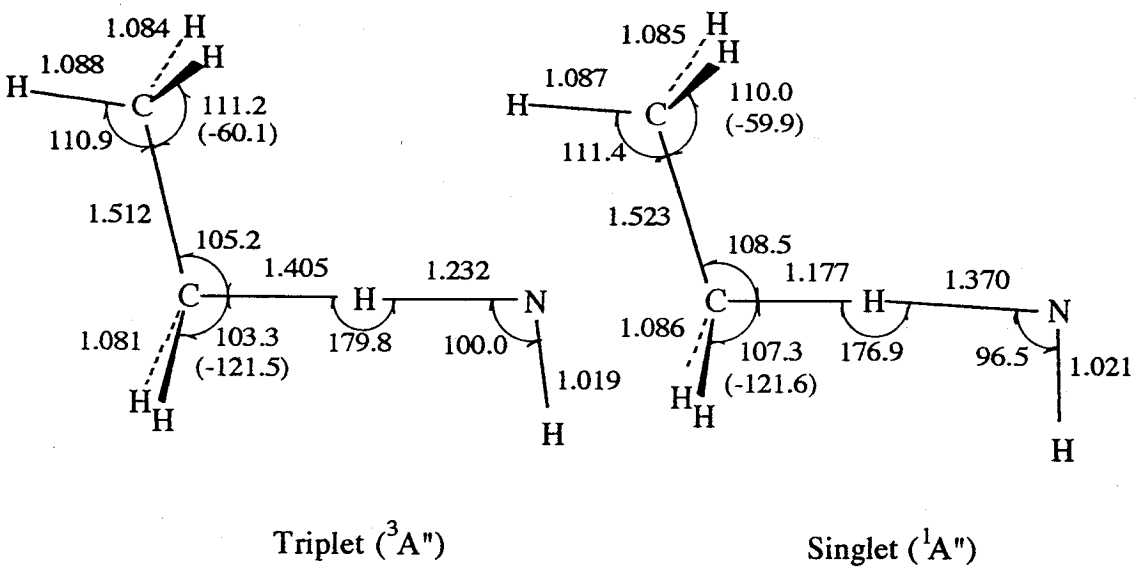

Figure 3. Geometries optimized for the transition states of the hydrogen abstractions of NH($^3\Sigma^-$) and NH($^1\Delta$) from C_2H_6. The basis sets used are the 6-31G(d) functions.

Part II

Dynamism of the Reactions of Some Sulfur-Containing Molecules

Chapter 1

Ab Initio Study of the Bimolecular Homolytic Substitution (S_H2) Reactions of RSH (R = H, CH_3)

Mechanisms of the hydrogen abstraction and the radical substitution reactions of H_2S with some atomic radicals X (X = H, O, F) and those of CH_3SH with H have been investigated by *ab initio* molecular orbital calculations. For all the reaction systems studied, transition states were located at the HF/6-31G** level, whereas no adduct could be found. At the MRD-CI level using the 6-31G** plus the Rydberg *s* and *p* orbitals on sulfur, the activation energies of the homolytic substitution reactions $H_2S + X \rightarrow H + HSX$ are calculated to be 50, 127, and 104 kJ/mol, for X = H, O, and F, respectively. For the substitution reaction $CH_3SH + H \rightarrow CH_3 + H_2S$, the activation energy calculated is as low as 19 kJ/mol, which is even slightly lower than that for the abstraction $CH_3SH + H \rightarrow CH_3S + H_2$. The predicted prevalence of the homolytic substitution reaction of CH_3SH over the abstraction is qualitatively in harmony with observations.

1. Introduction

To clarify the mechanisms of the reactions of organic sulfur species is intriguing in relation to those of the oxygen homologs. It is known that the most dominant reaction of alcohol with a radical, for example, a hydrogen atom, is the hydrogen abstraction (reaction (1)). On the other hand, in the case of thiols, not only the abstraction but also the radical substitution forming R + H_2S can take place (reaction (2)) [1, 2].

$$ROH + H \longrightarrow RO + H_2 \quad (1)$$

$$RSH + H \longrightarrow RS + H_2 \quad (2a)$$

$$\longrightarrow R + H_2S \quad (2b)$$

Pryor and Guard [3] measured the relative rate constants for the reactions of aliphatic disulfides with phenyl radicals in the liquid phase. It was concluded that the reactions might proceed by the back-side-attack mechanism similar to the ionic S_N2 reactions.

$$RSSR + Ph \longrightarrow RS + PhSR \quad (3)$$

In general, substitution reactions can be further divided into the following two categories:

$$AB + C \rightarrow [A\text{--}B\text{--}C]^{\ddagger} \rightarrow A + BC \quad (4)$$

$$AB + C \rightarrow (A\text{-}B\text{-}C) \rightarrow A + BC \quad (5)$$

Reaction (4) is a direct substitution, which is in itself an elementary reaction (S_H2, bimolecular homolytic substitution), while reaction (5) should proceed stepwise (i.e., the addition and the subsequent bond scission). Such mechanisms as reaction (5) are generally possible when BC has an unsaturated bond. Moreover, if B has available low-lying *d* orbitals as in the case of the second-row elements, intermediacy of hypervalent adducts may be possible. In this point of view, the above reactions (2) and

(3) arouse particular interests, since it is the sulfur atom that is attacked by radicals.

MNDO calculations [5] have predicted that there are stable adducts on both the H_2S + H and CH_3SH + H reactions. They are, however, somewhat dubious on the ground of the general features [6] of hypervalent species, i.e.,

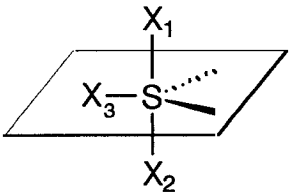

(a) The trivalent sulfur compounds (9-S-3) [7] should have the pseudo trigonal bipyramidal structures.

(b) The ligands which have large electronegativity must be present and are situated in the apical position to form such structures. For example, the experimental results [8] of ESR spectra have shown that the structures of sulfuranyl radicals do not have the C_{3v} but the C_{2v} symmetry, even while it has three identical F atoms. Theoretical treatments of SF_3 and SH_3 have been explored by Volatron et al.[9] by ab initio SCF and CI calculations. The results have shown that, while SF_3 is a stable adduct, SH_3 does not have a minimum but is a transition state of the H atom exchange reaction. In other words, it should correspond to a transition state of a bimolecular homolytic substitution (S_H2) of the reaction $H_2S + H' \rightarrow H + HSH'$.

In this paper, we examine the calculations of the reactions of hydrogen disulfide with some radicals (H, O, F) by using ab initio SCF and MRD-CI methods. The mechanisms of the reaction CH_3SH + H will be investigated in a similar manner, paying attention to the relative dominances of the abstraction and the substitution.

2. Method of calculations

All molecular structures, including those for transition states, were determined by the analytical gradient method [10]. These geometry calculations were first conducted at the 3-21G(*) [11] level. The 3-21G(*) calculations were followed by calculations of the 6-31G** [12] quality. The unrestricted Hartree-Fock (UHF) formalism was availed for all the radical species. The transition states located were verified by the vibrational analyses at the HF/6-31G** level.

All the SCF optimized structures were then subjected to the multi-reference double-excitation configuration interaction (MRD-CI) calculations. The table MRD-CI program furnished by Buenker [13,14] was used throughout. The configuration-selection and extrapolation routines were followed [15]. The maximal dimension of the configuration space used was up to 10,000. The extrapolated CI energies ($E_{T\to 0}$) were all subjected to the Langhoff-Davidson corrections [16], to estimate the full CI limit values (E_{CI}). At each MRD-CI calculation a small SD-CI calculation relative to the SCF ground state was first carried out. From the results of the SD-CI calculation, the configurations whose contributions $|C_i|^2$ to a state under consideration exceeded 0.3% were selected as reference configurations.

Two different basis sets were used in the CI calculations. One was the 6-31G** functions, as has been used in the geometry optimizations. The other was the 6-31G** sets augmented with the single Rydberg type s ($\zeta = 0.023$) and p ($\zeta = 0.020$) functions [17] on sulfur. We will refer to the latter basis sets as Ryd hereafter.

For the sake of comparison, the energies were further computed at the second-order (MP2) and fourth-order (MP4) perturbations in the single, double, triple, and quadruple excitations [18] approximations. All the perturbation calculations included the excitations of the valence orbitals alone.

3. Results

3.1. $H_2S + H$

This system may be the simplest type of reaction (2). In this case, reactions (2a) and (2b) can be represented as follows:

$$H_2S + H \longrightarrow SH + H_2 \qquad (6a)$$

$$\longrightarrow H + H_2S \qquad (6b)$$

Reaction (6a) is a hydrogen abstraction reaction to form SH and a hydrogen molecule. The potential energy surface of reaction (6b) is thermoneutral since the entrance channel is identical to the exit one.

The geometries obtained at the UHF/6-31G** of these transition states (TS) are illustrated in Figure 1-(a). The transition state (**1**) of the abstraction (reaction (6a)) is planar, and the angle of $<H^3H^2S$ is almost 180° (175.6°). The S-H^2 bond of **1** is a relatively long, being 1.480 Å, while the H^2-H^3 bond is nearly equal to that of H_2. It has one imaginary vibrational frequency ($2280i$ cm^{-1}) in the anti-symmetric stretching mode, i.e., the reaction coordinate. By contrast, in the substitution reaction, the transition state (**2**) is not planar as is shown in Fig. 1. It has an almost T-shaped C_s symmetry as has been proposed by previous workers [8] using the 4-31G basis sets augmented with polarization and diffuse orbitals on sulfur. The two longer S-H^2 bonds are 1.504 Å, in length while the remainder is 1.322 Å long. It should be pointed out that our UHF/6-31G** calculation of **2** gave the T-shaped structure similar to their result in spite of the absence of the diffuse functions on sulfur. The imaginary frequency of **2** is calculated to be $1246i$ cm^{-1}.

The relative energies obtained at various levels of theory are listed in Table 2. At the HF/6-31G** level, the activation energy of the abstraction is $\Delta E^{\ddagger}$ = 52 kJ/mol and that of the substitution is 90 kJ/mol. As the level of the perturbation effect became higher, the activation barriers tended to be lower. At the MP4(SDTQ)/6-31G** level, the activation energies are both reduced to 31 and 59 kJ/mol, respectively. The Rydberg type orbitals on the sulfur atom do not affect the relative energies in this system. It can be seen that the abstraction path (reaction (6b)) is energetically more favorable than the substitution pathway at any level of theory. However, it should be noticeable that the substitution channel can also exist with a considerably small barrier when any level of correlation effects is included. At the highest level of the present calculations (CI/Ryd//UHF/6-31G**), the calculated activation barriers $\Delta E_{CI}^{\ddagger}$ are 15 for the abstraction and 50 kJ/mol for the substitution, respectively. When the vibrational

zero-point energy corrections at the SCF level are taken into account, the energies are changed to 12 and 51 kJ/mol, respectively. Recently, Yoshimura et al. [19] investigated reaction (6a) by shock tube experiments and also theoretically. In their best results at the PMP4(SDTQ)/6-311G**//MP2/6-31G** level, the activation energy was $E_0 = 17$ kJ/mol. They concluded that the theoretical rate constant calculated using this value is much lower than the experimental value at $T = 293$ K. They noted that the best fit of calculations to experiments was attainable when the E_0 value of 13 kJ/mol was used. The activation energy E_0 = 12 kJ/mol obtained by our CI calculation agrees reasonably well with the proposed value.

3.2. $H_2S + O(^3P)$

The reaction of H_2S with the ground-state oxygen atom has been studied extensively by a number of kineticists [20]. Bulk studies [21] have shown that reaction (7a) is the main channel, while the pathway leading to HSO (reaction (7b)) was estimated to account for less than 20% of the overall reaction yield. Several groups [22] have investigated the reaction using the molecular beam technique, and found that the HSO product scattering favors the backward hemisphere. Moreover, the high translational product energy observed suggest that reaction (7b) must be a direct process.

$$H_2S + O \longrightarrow SH + OH \qquad (7a)$$

$$\longrightarrow H + HSO \qquad (7b)$$

Judging from the features described above for the hypervalent species, one can expect that the adduct may be possible, if the O atom attacks H_2S from the back side of one of the S-H bond.

The optimized structures of the transition states are shown in Fig. 2. In this case, there are two different transition states for the abstraction. One is the $^3A'$ state while the other, the $^3A''$ state. Since the total energies are little different from each other, we here

deal with only the $^3A'$ state. The transition state (**3**) of abstraction is planar, and the O-H^2 and S-H^2 bond lengths are 1.209 Å and 1.562 Å, respectively. Contrary to the H_2S + H system, the transition state (**4**) of the substitution is planar, and the electronic state is $^3A''$. In the UHF description, one α spin is localized on the O *p* orbital perpendicular to the symmetry plane, and the other exist on the in-plane orbital spread in the direction of the H^2-S-O axis. We also tried to calculate with a different initial geometry to search for another possible optimum geometry. Thus, the geometry of the singlet sulfoxide, H_2SO was selected for the triplet calculation to optimize the triplet adduct geometry under the C_s restriction. However, the geometry has led only to the C_{2v} symmetric transition state corresponding to the exchange of the two hydrogens (Scheme I).

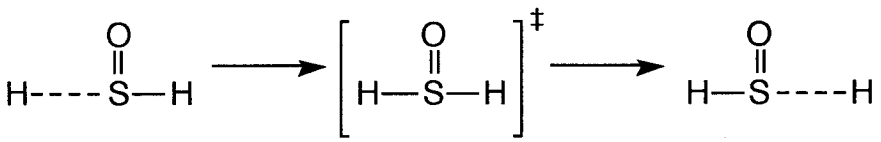

(Scheme I)

The activation energies and the relative energies to H_2S + O are listed in Table 2. At the HF/6-31G** level, the calculated activation energy of reaction (7a) is $\Delta E^{\ddagger}$ = 125 kJ/mol. By contrast, that of the substitution channel is $\Delta E^{\ddagger}$ = 221 kJ/mol. As the levels of the correlation effect become higher, both of the energies decrease. At the highest levels (MRD-CI/Ryd) of the present calculations, $\Delta E_{CI}^{\ddagger}$ for the abstraction is 77 kJ/mol and that for the substitution is 127 kJ/mol, respectively.

3.3. H_2S + F

The reaction will be represented as

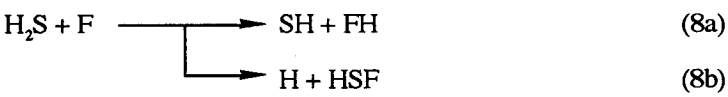

(8a)

(8b)

in this case. Reaction (8a) is known as a conventional source for the SH radial beam [23]. Although earlier workers [24] have mentioned the possibility of the pathway (8a), reaction (8b) has never been identified yet.

The optimized TS structures obtained are shown in Fig. 3. The geometry of the transition state (**5**) of the abstraction is similar to the structures of **1** and **3**, the H^2-F bond length being 1.245 Å. There exist only one imaginary frequency ($3092i$ cm^{-1}) at the UHF/6-31G** level. As in the case of **2**, the substitution TS (**6**) does not have the C_s symmetry. It has one imaginary frequency, being $937i$ cm^{-1}. The S-H^2 bond is comparatively long, being 1.942 Å.

The total energies obtained are listed in Table 3. Note that the energies of **5** are slightly lower than that of the reactant (H_2S + F) at the PMP2 level based on both the 6-31G** and the Ryd basis sets. At the MRD-CI/Ryd level, the activation energy is calculated to be $\Delta E_{CI}^{\ddagger}$ = 2.0 kJ/mol. Furthermore, at the same level, the relative energy of **6** against H_2S + F is calculated to be $\Delta E_{CI}^{\ddagger}$ = 104 kJ/mol, which is slightly lower than that of HSF + H ($\Delta E_{CI}^{\ddagger}$ = 123 kJ/mol). Since we have used the SCF geometries to calculate the CI energy, the geometry of **6** at the CI level may well be somewhat different from the SCF structure.

3.4 . CH_3SH + H

Amano et al.[2] measured the rates of the reactions

$$CH_3SH + H \xrightarrow{k_{9a}} CH_3S + H_2 \quad (9a)$$

$$CH_3SH + H \xrightarrow{k_{9b}} CH_3 + H_2S \quad (9b)$$

$$k_{9a} = 2.9 \times 10^{13} \exp(-10900/RT)$$

$$k_{9b} = 0.69 \times 10^{13} \exp(-6990/RT)$$

by a discharge flow method at 310-480 K. It has been concluded from the product

distribution that about one half of the reaction proceeded by pathway (9b). The result is of particular interest since in this case the activation energy of the substitution is lower than that of the abstraction. Thus, the experimental activation energies are 10.9 and 6.99 kJ/mol for reactions (9a) and (9b), respectively.

Results of the SCF optimizations of the TS structures are shown in Fig. 4. Both the transition states are planar. The TS structure **8** for the substitution reaction is characterized by the remarkably long C-S bond, which is as long as 1.975 Å. The length of the S-H^2 bond opposite to the C-S bond is 1.660 Å. Other structural parameters for both the transition states are little altered from those of CH_3SH.

The relative energies are shown in Table 5. At the HF/6-31G** level, the activation energies of abstraction and substitution are 50 and 69 kJ/mol, respectively. Even at the MP4/6-31G**, the advantage of abstraction is qualitatively not changed. Interestingly enough, the CI results are contrary to the SCF and MP results. The activation energy calculated for the substitution is apparently *lower* than that for the abstraction. Thus, the activation energies for the abstraction and the substitution are now 32 and 19 kJ/mol, respectively. The results of the CI calculations are qualitatively in line with the experimental results reported by Amano et al.[2].

4. Discussion

First, we describe the term "S_H2" used in the present paper. It seems that there are some arbitrariness in the definition of S_H2 reactions. In this paper, we have used the term "S_H2" as the type of reaction (4) and distinguished it explicitly from the two-step reaction (5) (addition followed by bond scission). The term "S_H2 reaction" has already been used in a review [25] which, however, treated both the reactions as the S_H2 type. Kinetically, so long as the rate-determining step is the initial addition, the rates of reaction (5) as well as reaction (4) will indicate the second-order profiles. However, from the consideration of the analogy with the ionic S_N2 (an elementary reaction, not

stepwise), the term "S_H2" should only be used to mean such a type as reaction (4).

As has been demonstrated above, there also exist direct substitution reactions in all the reaction systems of $H_2S + H$, $H_2S + O$, $H_2S + F$, and $CH_3SH + H$ beside the hydrogen abstraction reactions. In the case of $CH_3SH + H$ in particular, the barrier height of substitution is shown to be low enough to permit it to compete with the hydrogen abstraction.

The kinetic studies by Amano et al.[2] have shown that the substitution reaction (9b) to form $CH_3 + H_2S$ is even more advantageous than the hydrogen abstraction (9a). The observed activation energies were 10.9 and 7.0 kJ/mol for the abstraction and the substitutions, respectively. By using the results of MNDO calculations, they have proposed that the substitution reaction will take place via an initial formation of the metastable intermediate RSH_2 with a considerably low barrier .

In our calculations, however, such a trivalent adduct could not be found on the potential energy surface of the $CH_3SH + H$ system. Instead, a pathway for the direct S_H2 reaction giving the same product mixtures is found. Besides, the activation energy obtained for the substitution is clearly lower than that for the abstraction at the CI level. The results corroborates the experimental kinetic results.

In the case of $H_2S + O(^3P)$, the abstraction channel of $H_2S + O$ is thought to be that of the H-L-H (heavy-light-heavy) type, whose skew angle is generally so narrow that one must necessitate to know its dynamics in order to get more reliable image of it. Moreover, one must consider not only the triplet-state surface but also the excited singlet-state, since $O(^1D)$ lies only about 190 kJ/mol above the triplet state. In the next chapter, we will describe the potential energy surfaces of the reactions of H_2S with $O(^1D)$, to compare between the triplet and singlet surfaces in detail.

5. Conclusions

It was found that there exist the pathways of the direct substitution reactions of H_2S

and CH_3SH with some atomic radicals (H, O, F) with the comparatively low activation barriers. In the case of CH_3SH + H, the substitution is more favorable than the abstraction. The results confirm the experimental results by reported previous workers.

References

[1] O. Horie, J. Nishino and A. Amano, Int. J. Chem. Kinet., **10**, 1043 (1978); T. Kamo, J. Tang, M. Yamada and A. Amano, *Nippon Kagaku Kaishi*, 688 (1987).

[2] A. Amano, M. Yamada K. Hashimoto and K. Sugiura, Nippon Kagaku Kaishi, 385 (1983).

[3] W. A. Pryor and H. Guard, J. Am. Chem. Soc., **86**, 1150 (1964).

[4] E. L. Eliel, in *Steric Effects in Organic Chemistry*, John Wiley and Sons, Inc., New York, 1956, pp. 142.

[5] K. Hashimoto and M. Yamada, Nippon Kagaku Kaishi, , 678 (1983); T. Kamo, M. Yamada, J. Tang and A. Amano, unpublished work.

[6] J. I. Musher, Angew. Chem. Int. Ed. Engl., **8**, 54 (1969).

[7] C. W. Perkins, J. C. Martin, A. J. Arduengo, W. Lau, A. Alegria, and J. K. Kochi, J. Am. Chem. Soc., **102**, 7753 (1980).

[8] J. R. Morton, K. F. Preston and S. J. Strach, J. Chem. Phys. **69**, 1392 (1978).

[9] F. Volatron, A. Demolliens, J-M Lefour and O. Eisenstein, Chem. Phys. Letters, **130**, 419 (1986).

[10] M. J. Frisch, J. S. Binkley, H. B. Schlegel, K. Raghavachari, C. F. Melius, R. L. Martin, J. J. P. Stewart, F. W. Bobrowicz, C. M. Rohlfing, L. R. Kahn, D. J. DeFrees, R. Seeger, R. A. Whiteside, D. J. Fox, E. M. Fleuder, S. Topiol and J. A. Pople, GAUSSIAN 86, Carnegie-Mellon Quantum Chemistry Publishing Unit. Pittsburgh (1984), IMS version registered by N. Koga, S. Yabushita, K. Sawabe and K. Morokuma.

[11] W. J. Pietro, M. M. Francl, W. J. Hehre, D. J. DeFrees, J. A. Pople and J. S. Binkley, J. Am. Chem. Soc., **104**, 5039 (1982).

[12] W. J. Hehre, L. Radom, P. v. R. Schleyer and J. A. Pople, *Ab Initio Molecular Orbital Theory*, Wiley, New York, pp. 82 (1986).

[13] R. J. Buenker, *Studies in Physical and Theoretical Chemistry*, vol. 21, R. Carbo, ed., Elsevier, Amsterdam,pp17-34 (1982).

[14] R. J. Buenker, R. A. Phillips, J. Mol.Struct. (Theochem), **123**, 291 (1985).

[15] R. J. Buenker, S. D. Peyerimhoff, Theor. Chim. Acta. **35**, 33 (1974).

[16] S. R. Langhoff, E. R. Davidson, Int. J. Quant. Chem., **8**, 61 (1974).

[17] T. H. Dunning, and P. J. Hay, in *Modern Theoretical Chemistry*, vol. 3, H. F. Schaefer III, ed., Plenum Press, New York, pp.1-27 (1977).

[18] C. Mϕller, M. S. Plesset, Phys. Rev., **46**, 618-622 (1934). For a review of modern applications, see: J. A. Pople, Ber. Bunsenges. Phys. Chem. **86**, 806 (1982).

[19] M. Yoshimura, M. Koshi, H. Matsui, K. Kamiya, and H. Umeyama, Chem. Phys. Letters, **189**, 199 (1992).

[20] G. Liuti, S. Dondes, and P. Harteck, J. Am. Chem. Soc., **88**, 3212 (1966); A. Sharma, J. P. Padur, and P. Warneck, J. Phys. Chem., **71**, 1602 (1967); D. A. Whytock, R. B. Timmons, J. H. Lee, J. V. Michael, W. A. Payne, and L. J. Stief, J. Chem. Phys., **65**, 2052 (1976).

[21] D. L. Singleton, G. Paraskevopoulos, and R. S. Irwin, J. Phys. Chem., **86**, 2605 (1982).

[22] R. Grice, Chem. Soc. Rev., **11**, 1 (1982); A. R. Clemo, F. E. Davidson, G. L. Duncan, and R. Grice, Chem. Phys. Letters, **84**, 509 (1981); N. Balucani, L. Beneventi, P. Casavecchia, D. Stranges, and G. G. Volpi, J. Chem. Phys., **94**, 8611 (1991).

[23] for example, T. Kasai, K. Ohashi, H. Ohoyama and K. Kuwata, Chem. Phys. Letters, **127**, 581 (1986).

[24] R. L. Williams and F. S. Rowland, J. Phys. Chem., **77**, 301 (1973).

[25] M. L. Poutsma, in *Free Radicals*, vol. 2, J. K. Kochi, ed., John Wiley and Sons, New York, N. Y., pp. 113 (1973).

Table 1. Relative energies (kJ/mol) calculated at various levels for the H_2S + H system

Methods	Relative Energies (kJ/mol)[a]			
	H_2S + H	TS(abst.)	TS(subst.)	SH + H_2
HF/6-31G**	(0)	52	90	-70
MP2/6-31G**	(0)	38	67	-58
PMP2/6-31G**	(0)	26	52	-62
MP4(SDTQ)/6-31G**	(0)	31	59	-70
CI(full)/6-31G**	(0)	14	49	-58
HF/Ryd	(0)	51	89	-69
MP2/Ryd	(0)	37	66	-58
PMP2/Ryd	(0)	24	51	-62
MP4(SDTQ)/Ryd	(0)	29	57	-70
CI(full)/Ryd	(0)	15	50	-54

a Relative to H_2S + H.

Table 2. Relative energies (kJ/mol) calculated at various levels for the H_2S + O system

Methods	Relative Energies (kJ/mol)[a]				
	H_2S + O	TS(abst.)	TS(subst.)	SH + OH	HSO + H
HF/6-31G**	(0)	125	221	5	169
MP2/6-31G**	(0)	64	97	-38	35
PMP2/6-31G**	(0)	47	82	-42	30
MP4(SDTQ)/6-31G**	(0)	62	101	-31	52
CI(full)/6-31G**	(0)	77	139	-19	37
HF/Ryd	(0)	123	219	6	168
MP2/Ryd	(0)	60	94	-38	33
PMP2/Ryd	(0)	43	78	-42	28
MP4(SDTQ)/Ryd	(0)	57	97	-30	50
CI(full)/Ryd	(0)	77	127	-18	20

a Relative to H_2S + O.

Table 3. Relative energies (kJ/mol) calculated at various levels for the H_2S + F system

Methods	Relative Energies (kJ/mol)[a]				
	H_2S + F	TS(abst.)	TS(subst.)	SH + HF	HSF + H
HF/6-31G**	(0)	85	179	-105	153
MP2/6-31G**	(0)	6	57	-183	45
PMP2/6-31G**	(0)	-14	47	-184	48
MP4(SDTQ)/6-31G**	(0)	7	75	-164	68
CI(full)/6-31G**	(0)	3	150	-150	125
HF/Ryd	(0)	84	177	-105	153
MP2/Ryd	(0)	4	54	-183	44
PMP2/Ryd	(0)	-15	44	-184	46
MP4(SDTQ)/Ryd	(0)	5	72	-164	67
CI(full)/Ryd	(0)	2	104	-149	123

a Relative to H_2S + F.

Table 4. Relative energies (kJ/mol) calculated at various levels for the $CH_3SH + H$ system

Methods	Relative Energies (kJ/mol)[a]				
	$CH_3SH + H$	TS(abst.)	TS(subst.)	$CH_3S + H_2$	$CH_3 + H_2S$
HF/6-31G**	(0)	50	69	-80	-85
MP2/6-31G**	(0)	34	59	-69	-44
PMP2/6-31G**	(0)	22	40	-73	-49
MP4(SDTQ)/6-31G**	(0)	27	48	-82	-59
MRD-CI/6-31G**	(0)	-29	-13	-91	-86
HF/Ryd	(0)	49	68	-80	-85
MP2/Ryd	(0)	33	56	-69	-44
PMP2/Ryd	(0)	20	38	-73	-49
MP4(SDTQ)/Ryd	(0)	25	45	-82	-59
MRD-CI/Ryd	(0)	32	19	-93	-90

a Relative to $CH_3SH + H$.

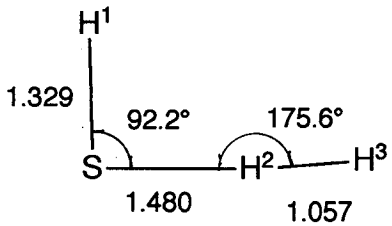

1

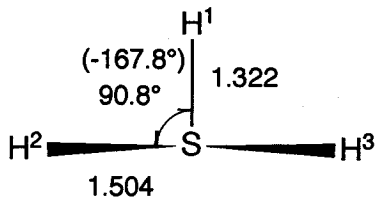

2

Figure 1. Optimized geometries for the transition states. The bond lengths are given in units of Å. The entry given in parentheses indicates the dihedral angle $\phi(H^3SH^1H^2)$. **1**, reaction (6a); **2**, reaction (6b).

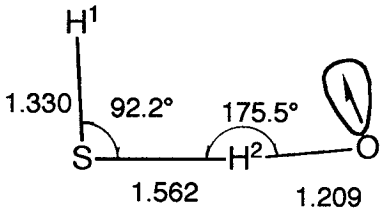

3 (^{3}A')

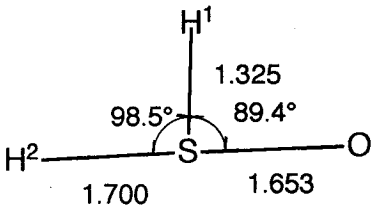

4

Figure 2. Optimized geometries for the transition states. The bond lengths are given in units of Å. **3**, reaction (7a); **4**, reaction (7b).

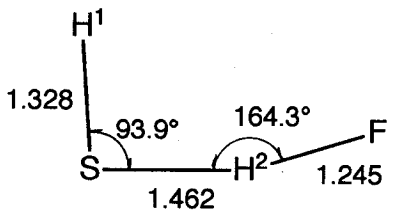

5

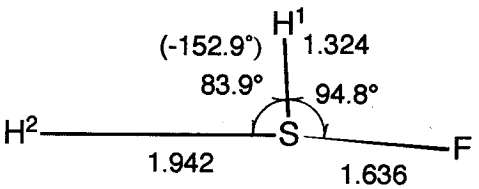

6

Figure 3. Optimized geometries for the transition states. The bond lengths are given in units of Å. The entry given in parentheses indicates the dihedral angle $\phi(FSH^1H^2)$. **5**, reaction (8a); **6**, reaction (8b).

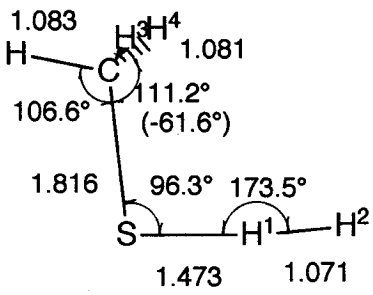

7

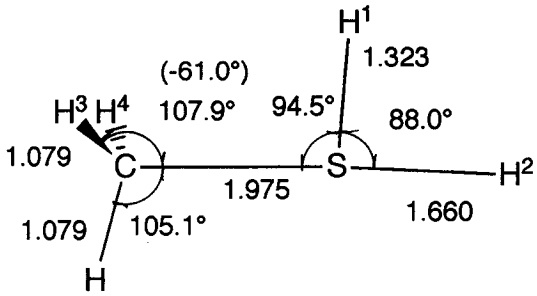

8

Figure 4. Optimized geometries for the transition states. The bond lengths are given in units of Å. The entries given in parentheses indicate the dihedral angles $\phi(H^3CSH^1)$. **7**, reaction (9a); **8**, reaction (9b).

Chapter 2

Potential Energy Surfaces of the Reactions of $H_2S + O(^3P, ^1D)$

Dynamical mechanisms of the reactions of H_2S with the oxygen atom in the ^1D and ^3P states have been investigated by ab initio SCF and MRD-CI calculations. The basis functions used are the 6-31G(*d*, *p*) sets throughout. The mechanism of the formation of HSO + H in the reaction of $O(^3P)$ is discussed from the standpoint of the direct bimolecular substitution. On the singlet surface, the reaction proceeds via an initial association giving H_2SO followed by the decomposition into HSO + H either by the H-S bond scission or by the isomerization into HSOH, which suffers the decomposition of the O-H bond. The activation barrier $\Delta E^{\ddagger}$ of the direct substitution is calculated to be too high on the triplet surface; the process may involve the interconversion to the singlet surface. Recent experimental data are discussed in the light of the theoretical results obtained.

1. Introduction

In chapter 1, the possible mechanisms of the reactions for H_2S and CH_3SH with some atomic radicals have been discussed. It was found that there exist the pathways of the direct S_H2 reactions (reaction (2)) of H_2S with X (X = O, H, F), while more favorable is the hydrogen abstraction (reaction (1)).

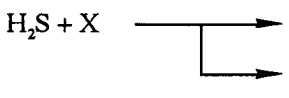

$$H_2S + X \longrightarrow SH + XH \quad (1)$$

$$\longrightarrow H + HSX \quad (2)$$

The reaction $H_2S + O(^3P)$ is the most interesting of the series of the reactions because previous workers [1] have suggested that the type of reaction (2) also exists, possibly proceeding via an adduct to give the products H + HSO eventually (reaction (4)). Several groups [2] have investigated the reaction using the molecular beam technique and concluded that reaction (4) giving the HSO product is a direct step without an intermediacy of the adduct.

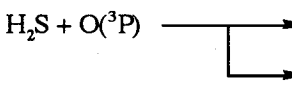

$$H_2S + O(^3P) \longrightarrow SH + OH \quad (3)$$

$$\longrightarrow H + HSO \quad (4)$$

Incidentally, since $O(^1D)$ lies only about 190 kJ/mol above the triplet state, not only the triplet but also the singlet surface may participate during the course of the reaction. In this point of view, information of the singlet surface for the reaction $H_2S + O(^1D)$ is necessary to understand the dynamism of the overall $H_2S + O(^3P)$ reactions.

Studies of the kinetics and mechanism of the reaction of $H_2S + O(^1D)$ have rather been limited as compared to the triplet case. The reaction may proceed with no barrier as in the cases of many other $O(^1D)$ reactions, giving sulfoxide H_2SO (**1**) in this case. Theoretically, Sola et al. [3] have studied the isomerization of **1** to **2** at the RHF level

using 6-31G(*d*) and 6-31G(*d*, *p*) basis sets, to investigate the effect of the optimization of polarization function exponents. Another theoretical study [4] treating the relative energies of **1**, **2**, and HSO + H by CI calculations is available in the literature. However, there is no study so far, which treats the overall profiles of the reactions of both $O(^3P)$ and $O(^1D)$ with H_2S, including isomerization of **1** into **2**.

The primary objective of this work is to elucidate the potential energy surfaces of the reactions of H_2S with $O(^1D)$ as well as $O(^3P)$, to compare between the triplet and the singlet surfaces. The isomerization of **1** into **2** are also treated at the same level.

2. Method of calculations

Geometry optimizations of both the singlet and triplet states were carried out with HF level employing the 6-31G(*d*, *p*) [5] basis set. For open-shell species, the unrestricted Hartree-Fock (UHF) formalism was used. The Gaussian 86 program package [6] was used for these purposes. In order to verify the character of the geometries, the vibrational analyses were undertaken by use of analytical second energy derivertives.

The transition states (TS) as well as the other stationary points obtained were then subjected to the multi-reference double excitation (MRD) configuration interaction (CI) computations. The Table MRD-CI program furnished by Buenker was used.[7-9] The final CI results (E_{CI}) were obtained using the configuration selection routine, the energy extrapolation, and the Davidson-Langhoff correction [10] as has already been described.

3. Results

3.1. Singlet States

It is presumed intuitively that the primary step of the reaction between H_2S and

$O(^1D)$ proceeds by an initial addition, giving a stable molecule H_2SO (reaction (4)).

$$H_2S + O(^1D) \longrightarrow H_2SO \qquad (4)$$

The adduct sulfoxide (**1**) may further isomerize into HSOH (**2**) by a 1, 2-hydrogen migration or suffer an S-H bond cleavage, giving HSO + H.

$$\begin{array}{lll} H_2SO & \longrightarrow & HSOH \qquad (5) \\ \mathbf{1} & & \mathbf{2} \\ & \longrightarrow & HSO + H \qquad (6) \end{array}$$

Moreover, in view of the open-shell character for $O(^1D)$, the direct abstraction

$$H_2S + O(^1D) \longrightarrow [HS\text{--}H\text{--}O]^{\ddagger} \longrightarrow SH + OH \qquad (7)$$

is also conceivable.

Figure 1 shows the geometries for **1**, **2**, and the transition state (TS1) of the isomerization process of **1** to **2**. The SCF optimized structure of TS1, as well as the geometries of H_2SO and HSOH, has already been reported by Sola et al.[3]. Since they did not give vibrational frequencies, the frequencies calculated here are listed in Table 1. The transition state (TS1) has one imaginary frequency, being $2028i$ cm^{-1}. In Fig. 2, the transition state (TS2) of the abstraction (reaction (7)) is illustrated. The transition state (TS2) for the abstraction has the C_s symmetry, the angle of <OHS being almost 180° as is usually the case. It also has one imaginary frequency, which is calculated to be $2948i$ cm^{-1}.

For the SCF optimized geometries, the MRD-CI calculations have been carried out. The results are summarized in Table 2. At the SCF level, **2** is 144 kJ/mol more stable than **1**, and the activation energy for reaction (5) is calculated to be $\Delta E^{\ddagger} = 216$ kJ/mol. At the CI level, the relative energy between **2** and **1** is reduced to 139 kJ/mol, and the

activation energy for the isomerization is 172 kJ/mol. When corrections for the vibrational zero-point energy at the SCF level are included, the relative energy between **1** and **2** comes out to be ΔE_0 = 136 kJ/mol, and the activation energy for the process **1**→**2** is reduced to $\Delta E_0^{\ddagger}$ = 159 kJ/mol. The relative energy between H_2S + $O(^1D)$ and **1** is calculated to be 323 kJ/mol at the CI level, which is reduced to 304 kJ/mol by the zero-point corrections. The activation energy for the abstraction (TS2) is lower than H_2S + $O(^1D)$. This may be due to the large difference between the SCF and CI geometries.

Reaction (4) may have a barrier when the electron correlation effects are included. In order to settle this question, we examined the geometry optimizations at various fixed S-O bonds from 1.48 Å(equiliblium S-O distance of H_2SO) to 2.8 Å, and the geometries are then subjected to CI calculations. The results are illustrated in Fig. 3. It is clearly shown there that the reaction has no activation barrier even at the CI level.

3.2. Triplet States

As described already in chapter 1, there are two different transition states for the abstraction. One is the $^3A'$ state while the other, the $^3A''$ state. For simplicity, only the $^3A'$ state was mentioned in chapter 1. In this section, we deal with both states in detail.

Figure 4 shows the TS geometries at the SCF for the abstraction on the triplet surfaces. As can be seen there clearly, the TS3 and TS4 have almost the same geometries.

In the same manner, the optimized geometries are then subjected to the MRD-CI calculations. The results are listed in Table 2. At the SCF level, the activation energies of TS3 and TS4 are 125 and 120 kJ/mol, respectively. The activation energy of TS4 is slightly lower than that of TS3, although the difference is only 5 kJ/mol. At the CI/6-31G(*d*, *p*) level, the energies are calculated to be $\Delta E^{\ddagger}$ = 76 and 72 kcal/mol, respectively. Moreover, the energies come out to be 66 and 62 kJ/mol, respectively. At any level of theory, TS4 is about 5 kJ/mol lower than TS3.

4. Discussion

The overall potential energy profiles for the reactions of $H_2S + O(^3P, ^1D)$ obtained by the present calculations are illustrated in Fig. 5. The experimental data [11] available are given in parentheses.

As demonstrated above, the reaction of H_2S with $O(^1D)$ proceed with virtually no barrier giving sulfoxide H_2SO (**1**). Moreover, because of its initial high energy, **1** will readily be decomposed into HSO + H or isomerize into **2**.

In the case of the reaction of H_2S with $O(^3P)$, the products HSO + H must be formed by the direct radical substitution (reaction (8)) or by conversion to the singlet surface.

$$H_2S + O(^3P) \longrightarrow (TS5)^{\ddagger} \longrightarrow HSO + H \qquad (8)$$

Very recently, the molecular beam experiments [12] have shown that the threshold collision energy E_C of the reaction (4) is 49 kJ/mol. If the reaction (4) proceeds by the mechanism of reaction (8), the calculated activation energy $\Delta E_0^{\ddagger} = 128$ kJ/mol is too high. By contrast, if the conversion between singlet and triplet surfaces occurs during the process, overall activation energy is 64 kJ/mol, which corresponds to the energy difference between $H_2S + O(^3P)$ and TS1. Qualitatively, this is in better agreement with the experimental results. However, this process can not explain the fact that the product HSO is scattered in the backward hemisphere.

It should be noted that there is some underestimation of the total energy of $O(^3P)$, since in the present calculation we have used the 6-componet *d* function as the polarization function of the O atom. By our experience in our CI calculations, the magnitude of the underestimation is roughly estimated to about 40 kJ/mol. Even when this correction is taken into account, the activation energy comes out to be $\Delta E_0^{\ddagger} = 88$ kJ/mol, a value which is still too high as compared with the net activation energy of 64 kJ/mol calculated for the process involving the triplet-to-singlet interconversion.

References

[1] G. Liuti, S. Dondes, and P. Harteck, J. Am. Chem. Soc., **88**, 3212 (1966); A. Sharma, J. P. Padur, and P. Warneck, J. Phys. Chem., **71**, 1602 (1967); D. A. Whytock, R. B. Timmons, J. H. Lee, J. V. Michael, W. A. Payne, and L. J. Stief, J. Chem. Phys., **65**, 2052 (1976); D. L. Singleton, G. Paraskevopoulos, and R. S. Irwin, J. Phys. Chem., **86**, 2605 (1982).

[2] R. Grice, Chem. Soc. Rev., **11**, 1 (1982); A. R. Clemo, F. E. Davidson, G. L. Duncan, and R. Grice, Chem. Phys. Letters, **84**, 509 (1981)

[3] M. Sola, C. Gonzalez, G. Tonachini, and H. B. Schlegel, Theor. Chim. Acta, **77**, 281 (1990).

[4] S. Besnainou and J. L. Whitten, J. Am. Chem. Soc., **102**, 7444 (1980).

[5] W. J. Hehre, L. Radom, P. v. R. Schleyer and J. A. Pople, *Ab Initio Molecular Orbital Theory*, Wiley, New York, pp. 82 (1986).

[6] M. J. Frisch, J. S. Binkley, H. B. Schlegel, K. Raghavachari, C. F. Melius, R. L. Martin, J. J. P. Stewart, F. W. Bobrowicz, C. M. Rohlfing, L. R. Kahn, D. J. DeFrees, R. Seeger, R. A. Whiteside, D. J. Fox, E. M. Fleuder, S. Topiol and J. A. Pople, GAUSSIAN 86, Carnegie-Mellon Quantum Chemistry Publishing Unit. Pittsburgh (1984), IMS version registered by N. Koga, S. Yabushita, K. Sawabe and K. Morokuma.

[7] R. J. Buenker, *Studies in Physical and Theoretical Chemistry*, vol. 21, R. Carbo, ed., Elsevier, Amsterdam, pp17 (1982).

[8] R. J. Buenker, R. A. Phillips, J. Mol.Struct. (Theochem), **123**, 291 (1985).

[9] R. J. Buenker, S. D. Peyerimhoff, Theor. Chim. Acta. **35**, 33 (1974).

[10] S. R. Langhoff, E. R. Davidson, Int. J. Quant. Chem., **8**, 61 (1974).

[11] M. W. Chase, Jr., C. A. Davies, J. R. Downey, Jr., D. J. Frurip, R. A. McDonald, and A. N. Syverud, *JANAF thermochemical Tables*, 3rd ed., National Bureau of Standards, Washington, D. C. (1985).

[12] N. Balucani, L. Beneventi, P. Casavecchia, D. Stranges, and G. G. Volpi, J. Chem. Phys., **94**, 8611 (1991).

Table 1. Calculated harmonic frequencies for H_2SO (**1**), HSOH(**2**), and TS1

	frequencies (cm^{-1})			E_Z(kJ/mol)[a]
H_2SO (**1**)	1091.4	1127.5	1197.2	61
	1396.6	2701.3	2710.8	
TS1	2027.6*i*	595.0	978.2	49
	1150.9	2672.2	2836.1	
HSOH (**2**)	514.3	868.4	1126.1	65
	1316.8	2867.6	4162.3	

a The zero-point energies at the HF/6-31G(*d*, *p*) level.

Table 2. Relative energies for **1**, **2**, and TS1 at the RHF and the CI level

	E_{SCF}(hartree)	E_{CI}(hartree)	Relative energies (kJ/mol)		
			SCF	CI	CI + vib[a]
$H_2S + O(^3P)$	-473.45896	-473.71324	(0)	(0)	(0)
$H_2S + O(^1D)$	.33163	.63348	99[b]	209	209
H_2SO (**1**)	.44508	.75664	36	-114	-95
TS1	.36314	.69128	252	58	64
HSOH (**2**)	.49999	.80977	-108	-253	-231
TS2 ($^1A''$)	.38892	.64572	184	177	167
TS3 ($^3A'$)	.41154	.68411	125	76	66
TS4 ($^2A''$)	.41329	.68571	120	72	62
TS5 ($^3A''$)	.37482	.66037	221	139	128
HSO + H	.39479	.69919	168	37	23
SH + OH	.45681	.72096	6	-20	-21
HOS + H	.40583	.68414	139	76	72

a Including the zero-point energy corrections at the HF/6-31G(*d*, *p*) level.

b $O(^1D)$ is calculated at the UHF level.

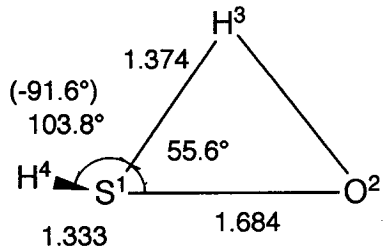

TS1

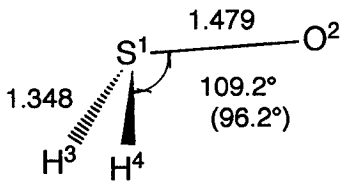

H_2SO (**1**)

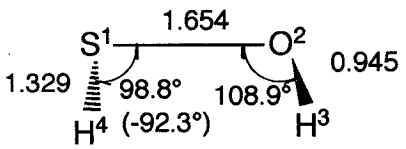

HSOH (**2**)

Figure 1. Optimized geometries of H_2SO (**1**), the transition state (TS1), and HSOH (**2**). The bond lengths are given in units of Å. The entries given in parentheses indicate the dihedral angles $\phi(H^4S^1O^2H^3)$.

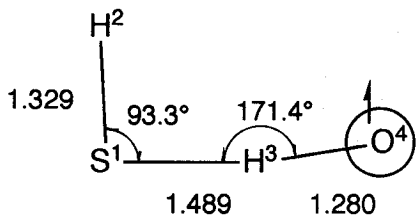

TS2 (^{1}A")

Figure 2. Optimized geometry of the transition state (TS2). The bond lengths are given in units of Å.

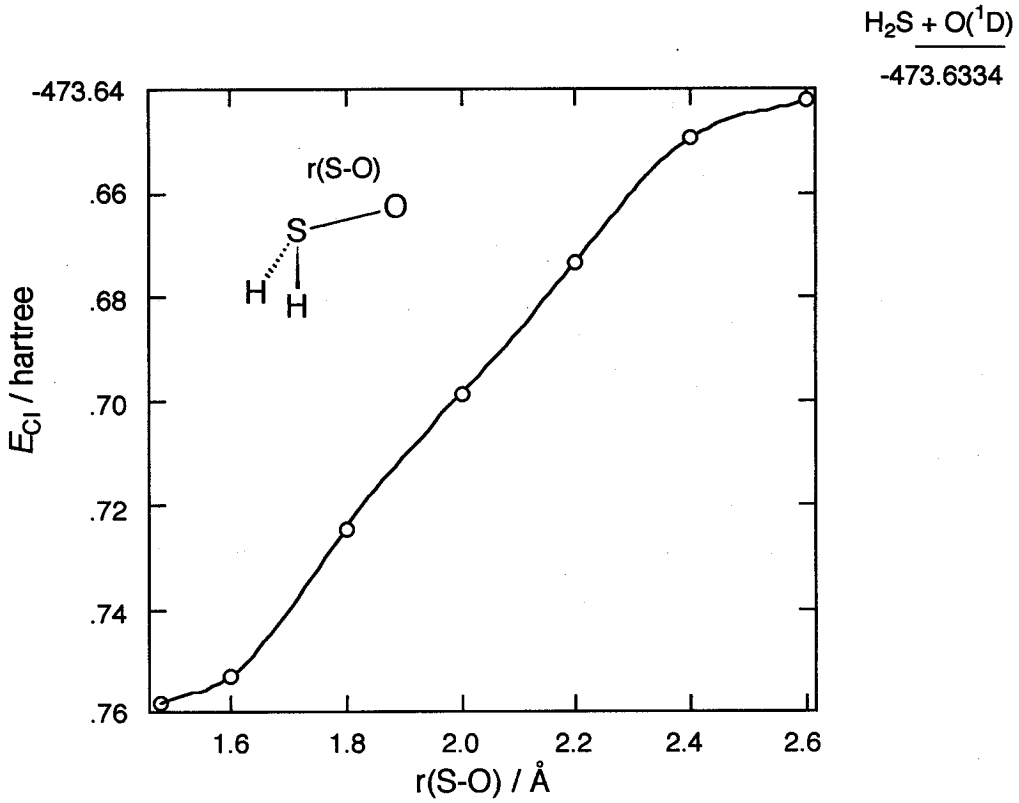

Figure 3. Potential energy curve calculated for the $H_2S + O(^1D)$ system.

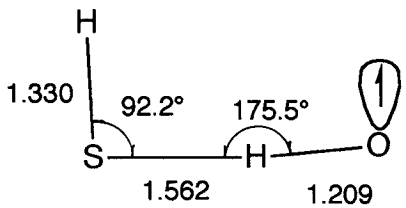

TS3 (^{3}A')

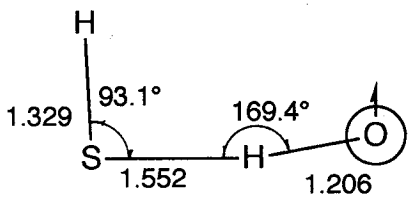

TS4 (^{3}A")

Figure 4. Optimized geometries of the transition states. The bond lengths are given in units of Å.

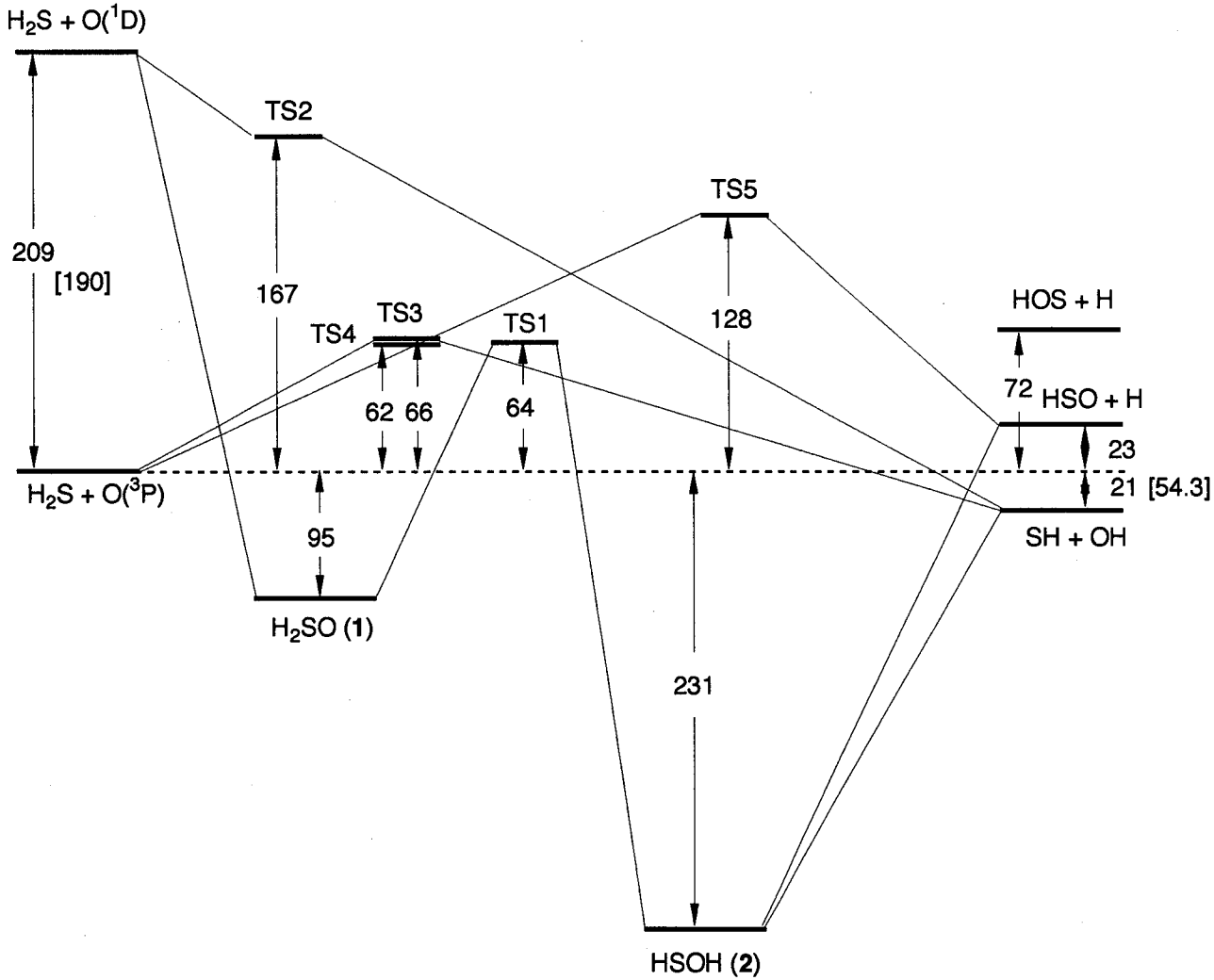

Figure 5. Potential energy profiles calculated for the H_2S + O system. The energy levels are based on the E_{CI} value including the zero-point energy corrections. Energy gaps shown are in units of kJ/mol.